TECHNISCHE
UNIVERSITÄT
MÜNCHEN

WALTHER - MEISSNER -
INSTITUT FÜR TIEF -
TEMPERATURFORSCHUNG

BAYERISCHE
AKADEMIE DER
WISSENSCHAFTEN

Impedance matching of metal powder filters for experiments with superconducting flux quantum bits

Bachelor's Thesis

Edwar Xie

Supervisor: Prof. Dr. Rudolf Gross

Munich, January 2011

Contents

List of Figures

Chapter 1

Motivation

Since years quantum mechanics has become more and more important in the focus of science. Granted the development of cryostats, which are able to cool down a sample to millikelvin - hence eliminate thermal noise -, quantum effects can be observed experimentally. Due to the high demands of quantum experiments regarding the absence of noise sources, shielding techniques are an essential part of the experimental setup. Measurements with superconducting circuits in a cryostat, which are very sensitive to electromagnetic high frequency noise, are required to be shielded. By coating the setup with sheet metal or Mu-metal, shielding can be achieved easily for every component except the wires connected to the circuit. Through this leak electromagnetic noise, such as the signal of a nearby radio station, may disturb the experiment. In order to eliminate this source of noise, high frequency filters, i.e., metal powder filters, are needed. Copper powder filters (CPF) or stainless steel powder filters (SSPF) are commonly used as lowpass filters in experiments with superconducting flux qubits. These are circuits fabricated on silicon chips and operated at millikelvin temperatures in the context of solid state quantum simulation and information processing. Such experiments often require current control pulses with rise times down to $\tau \simeq 1\,\mathrm{ns}$ while, at the same time, environmental current noise at frequencies larger than $1/\tau$ must be suppressed in order to observe quantum phenomena. For this purpose, SSPF are well suited because they combine an attenuation of more than 80 dB with a steep fall-off between passband and stopband (cf. Fig. 1.1).

By reason that the filters are positioned usually inside the cryostat close to the device under test, in former experiments CPF and SSPF have been characterized on the basis of their attenuation at various temperatures down to 4.2 K. Fukushima et al. also present another technique for filtering electromagnetic noise by using thermocoax filters with SMA connectors at both ends [1].

More generally powder filters with embedded capacitors as LC-filters have a lower cut-off frequency at about 1 MHz. Lukashenko et al. combine a reproducible low cut-off frequency with a compact design of the filters [2]. Instead of using a LC-filter Forn-Diaz et al. implemented a Josephson junction resulting in a squelch circuit. Signals with low amplitude are shorted by the squelch, whereas for strong signals the squelch is off and the powder filter attenuates the high frequencies [3]. Besides the principle of metal grains

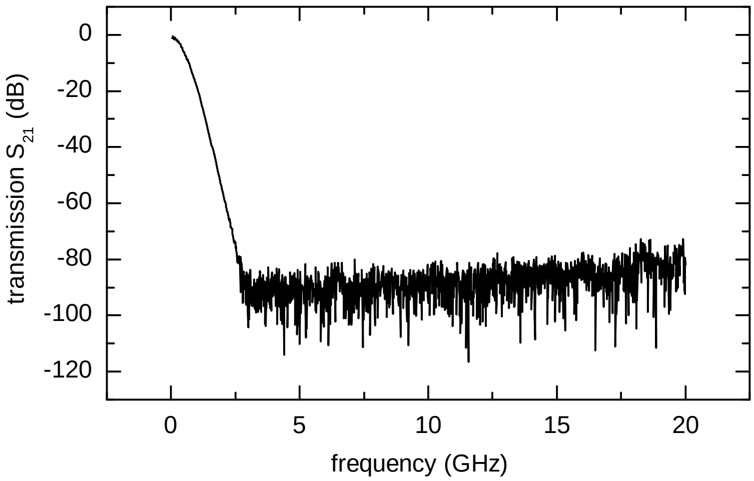

Figure 1.1: Attenuation of a SSPF with steep fall-off and constant attenuation

acting as resonant circuits and dissipating the energy of high frequency noise, there are approaches to use striplines [4] and twisted pairs of resistive wires [5].

Despise all these attempts on optimizing the filter quality in the stopband, an unchanged passband is even more relevant, because otherwise the measurement would be impaired. In this work, we concentrate on SSPF and address an aspect of fundamental importance in the microwave regime: impedance matching. On the one hand, attenuation is required for the high frequency noise, but on the other hand, the transmitted and measured signals should not be affected by the filter. For pulses with a gigahertz bandwidth, an SSPF with an impedance different from the $50\,\Omega$ standard used by the pulse sources creates ghost images due to multiple reflections. As a consequence, the pulse can be severely distorted. Although, for example, Gaussian shaped pulses are more tolerant with respect to this effect, the design of probe signals remains limited. For this reason, we characterize standard SSPF designs, improve them, and develop a technique for building $50\,\Omega$ matched SSPF without compromising their attenuation characteristics.

We will first investigate the conventional SSPF with SMA connectors on both sides by transmitting an arbitrary probe signal and by the use of TDR. The weak points in this particular design are going to be revealed and will be dealt with by changing essential parts of the filter. Specifically a simulation is made with ADS2009 in order to design a new type of filter, which is still based on the power absorption principle though.

Although our SSPF are completely characterized at room temperature, our impedance matching technique can be applied to cryogenic SSPF with no or minor technical changes. In this way, we remove the most critical obstacle for the shaping of control pulses in experiments on flux quantum circuits, paving the way for ambitious goals such as optimum control strategies on the one-nanosecond timescale for an improved fidelity of quantum gates with solid state circuits.

Chapter 2

Experimental techniques and microwave simulations

2.1 Design and fabrication of SSPF

In principle, a SSPF consists of enameled copper wire embedded in stainless steel powder, whose grains are isolated from each other by a thin oxide layer. In this way, microwave fields induce currents in each grain and the effective surface contributing to dissipation is large. Consequently, such fields are efficiently attenuated at least up to several tens of gigahertz. SSPF can have a steep filtering characteristic, for approximately 1m of copper wire the transmission typically drops from near unity to -80 dB within 2 GHz. To keep the filter compact and avoid noise from environmental electromagnetic fields, in our case the wire is wound in ∞-form around two rods made of a mixture of Stycast 1266 and stainless steel powder. In the following, we will refer to such a construction, which is shown in Fig. 2.1, as a ”core”. The core is placed in a copper or brass housing and the wire ends are equipped with SMA connectors (cf. Fig. 2.2).

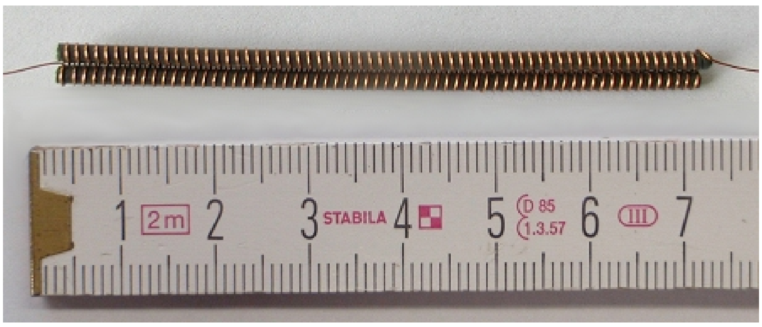

Figure 2.1: Core made of a Stycast and stainless steel powder mixture with 200 µm-diameter copper wire wound in ∞-form.

2.1.1 Filters with asymmetric SMA assembly

A very convenient way to fabricate a SSPF with two SMA connectors is to solder one connector to the core, insert the core into the housing, and glue the connector to the housing. In the next step, stainless steel powder is filled into the housing and the second connector is attached to the free end of the copper wire. During the filling process it is recommended to densify the powder by using a vibrating apparatus (cf. appendix Fig. A.1). Finally, the second connector is glued into the housing (cf. Fig. 2.2).

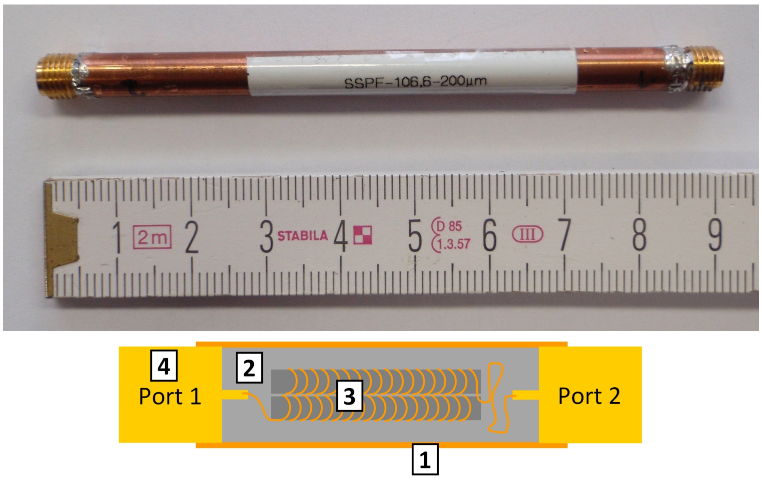

Figure 2.2: Filter with SMA connectors on both sides: One can see the [3] core in ∞-form inside the [1] copper casing with [2] densified stainless steel powder. [4] SMA connectors are pressed into the casing and sealed with Stycast. After that, additional solder was applied to provide a good grounding. Note that the wire at port 2 is longer due to the fabrication process. In the end each filter was labeled with important data, e.g. wire length and diameter. In this case it is a SSPF with 106.6 cm wire length and a 200 µm copper wire.

Due to this fabrication process these filters, which we refer to as ”type one” in the following, are inherently strongly asymmetric with respect to their reflection properties. The reason is that the wire at the second connector is surrounded mostly by Stycast, whereas the wire near the first connector is almost completely embedded in stainless steel powder.

2.1.2 Filters with symmetric SMA assembly

In the course of this work, we developed a symmetric SSPF with equal reflection properties at both connectors. Such an improved design is indispensable for controlling the wire-connector transition. In this design, the core is fixed inside the housing with a Teflon (thickness 2 mm) or Kapton disc (thickness 125 µm). The wire ends are fed through small holes in the center of the disc (cf. Fig. 2.3). Details of the fabrication procedure can be found in appendix A.

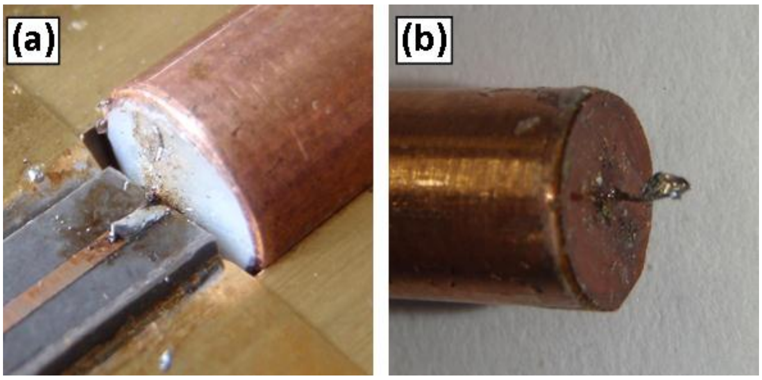

Figure 2.3: Filter with (a) a piece of Teflon pressed into the filter and the wire stub soldered onto a printed circuit board and (b) piece of Kapton foil glued onto the copper casing.

In order to guarantee a controlled transition from the copper wire ends and the SMA connectors, a 50 Ω-matched printed circuit board (PCB) is inserted in between. Finally, everything is placed inside a brass sample holder (cf. Fig. 2.4).

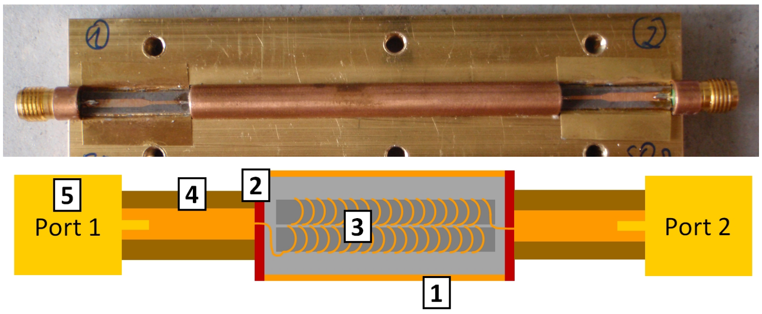

Figure 2.4: Sample holder for symmetric filters ([1] copper casing, [2] Kapton foil, [3] core in ∞-form): Two [4] printed circuit boards with [5] SMA connectors are attached to both ends of the filter. The lid of the sample holder (not shown) is fixed with screws.

2.2 Pulse transmission measurements

In flux qubit measurements, current pulses are used for control and readout. The typical rise time t_{rise} of such pulses is approximately 1 ns [6]. In many cases, frequencies above $1/t_{\mathrm{rise}}$ must be filtered efficiently. Hence, we can evaluate the performance of our SSPF by monitoring its effect on various pulses on an oscilloscope. The corresponding experimental setup is displayed in Fig. 2.5.

Gaussian shaped pulses have the advantage of remaining compact in frequency space (the Fourier transform of a Gaussian is a Gaussian). In contrast, rectangular pulses, where higher harmonics have a considerable spectral weight [7], act as a benchmark

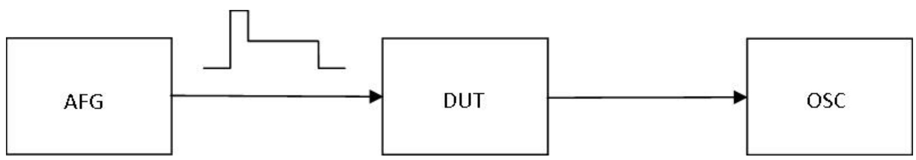

Figure 2.5: Setup for pulse transmission measurements. The pulse is created using a Tektronix AFG 3252 arbitrary function generator (AFG). The device under test (DUT) is the SSPF. The transmitted pulse is recorded with a LeCroy Wavemaster 8600A oscilloscope (OSC).

for the impedance matching. SSPF which leave these probe pulses undisturbed will ultimately be suitable for advanced qubit manipulation techniques such as optimal control [8]. Therefore we focus on the latter one in the course of this work. Typical examples are shown in Fig. 2.6.

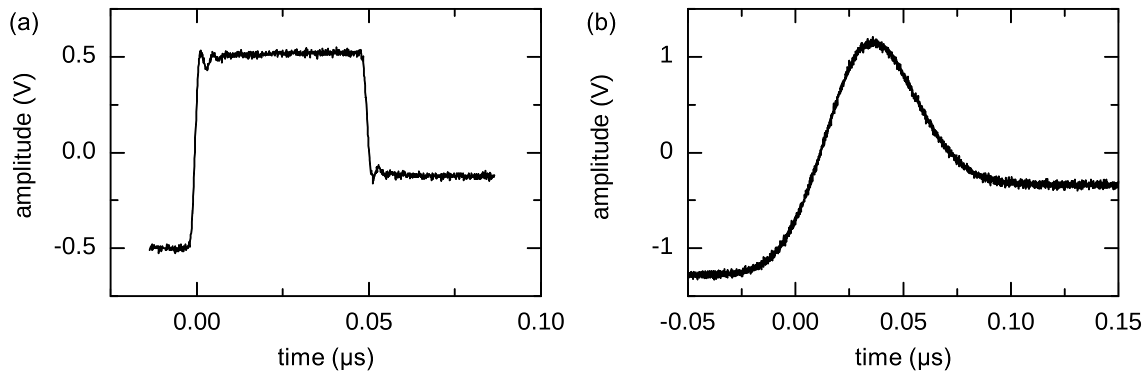

Figure 2.6: (a) rectangular pulse with 50 ns width and (b) Gaussian pulse with 50 ns FWHM. Both are followed by a hold level.

2.3 S-parameter measurements

Microwave devices are commonly characterized via their scattering or S-parameters. Their S-parameters characterize the transmission and reflection of a device and are the elements of the scattering matrix [1] [9]

$$S_{ij} = \left.\frac{V_i^-}{V_j^+}\right|_{V_k^+=0 \text{ for } k\neq j} . \tag{2.1}$$

V_j^+ is the voltage of the wave incident at port j of the device and V_i^- is the voltage of the wave reflected at port i. As we only look at devices with two ports, the scattering matrix reduces to

[1] S-parameters can be given in decibel (dB): S_{ij} in dB $= 20 \cdot lg(\text{linear } S_{ij})$.

- S_{11}, input port voltage reflection coefficient,
- S_{12}, reverse voltage gain/attenuation,
- S_{21}, forward voltage gain/attenuation and
- S_{22}, output port voltage reflection coefficient.

2.3.1 Vector network analyzer setup

Experimentally, the attenuation of the filters is determined using a network vector analyzer (VNA). A VNA generates a probe signal at one port and detects amplitude and phase of the components reflected from and transmitted through the device under test (DUT). This setup is shown schematically in Fig. 2.7.

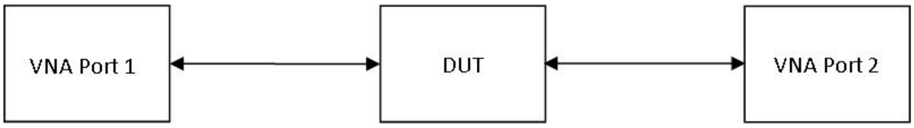

Figure 2.7: Setup for S-parameter measurements. The device under test (DUT) is inserted between the two ports of a HP 8722D or a Rohde & Schwarz ZVB vector network analyzer (VNA).

2.3.2 SSPF: Transmission/reflection/absorption model

The measured S-parameters characterize the performance of a device as a whole. In order to gain additional understanding of the inner structure of the SSPF, we introduce a simple transmission/reflection/absorption (TRA) model and discuss its consequences on the measured S-parameters. In this model, the SSPF has two reflection points (reflection coefficients Γ_1 and Γ_2; transmission coefficients T_1 and T_2), each located at the end of a purely absorptive body (absorption coefficient A) as shown in Fig. 2.8.

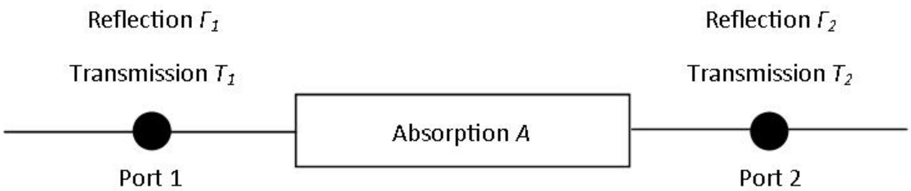

Figure 2.8: Simplified system to explain transmission and reflection.

Keeping in mind that $A\,,\Gamma_{1,2}\,,T_{1,2} < 1$ and $\Gamma_{1,2}^2 + T_{1,2}^2 = 1$, the power transmitted through the device is

$$\begin{aligned}
P_T &= \left\{\left[\sqrt{1-\Gamma_1^2}\cdot A\cdot\sqrt{1-\Gamma_2^2}\right]^2+\left[\sqrt{1-\Gamma_1^2}\cdot A\cdot\Gamma_2\cdot A\cdot\Gamma_1\cdot A\cdot\sqrt{1-\Gamma_2^2}\right]^2+...\right\}P_0\\
&= \left\{\sum_{n=0}^{\infty}\left[\sqrt{1-\Gamma_1^2}\cdot A^{2n+1}\cdot\Gamma_1^n\cdot\Gamma_2^n\cdot\sqrt{1-\Gamma_2^2}\right]^2\right\}P_0\\
&= \left\{(1-\Gamma_1^2)\cdot A^2\cdot(1-\Gamma_2^2)\sum_{n=0}^{\infty}\left[A^{2n}\cdot\Gamma_1^n\cdot\Gamma_2^n\right]^2\right\}P_0\\
P_T &= \left\{\frac{(1-\Gamma_1^2)\cdot A^2\cdot(1-\Gamma_2^2)}{1-(A^2\cdot\Gamma_1\cdot\Gamma_2)^2}\right\}P_0, \qquad (2.2)
\end{aligned}$$

where P_0 is the probe power. Equation (2.2) implies that we expect $S_{12}=S_{21}$ for the SSPF even in the case of different reflection coefficients $\Gamma_1\neq\Gamma_2$. Although the exact formula will change, this argument still holds for real device with possibly more reflection points because for a transmission the probe signal has to be reflected an even number of times.

The reflection coefficients, however will be different in general. We can see this from the power reflected at port 1:

$$\begin{aligned}
P_{R_1} &= \left\{\Gamma_1^2+\left[\sqrt{1-\Gamma_1^2}\cdot A\cdot\Gamma_2\cdot A\cdot\sqrt{1-\Gamma_2^2}\right]^2+...\right\}P_0\\
&= \left\{\Gamma_1^2+\sum_{n=0}^{\infty}\left[\sqrt{1-\Gamma_1^2}\cdot A^{2n+2}\cdot\Gamma_1^n\cdot\Gamma_2^{n+1}\cdot\sqrt{1-\Gamma_2^2}\right]^2\right\}P_0\\
&= \left\{\Gamma_1^2+(1-\Gamma_1^2)\cdot A^2\cdot(1-\Gamma_2^2)\cdot\Gamma_2^2\cdot\sum_{n=0}^{\infty}\left[A^{2n}\cdot\Gamma_1^n\cdot\Gamma_2^n\right]^2\right\}P_0\\
P_{R_1} &= \left\{\Gamma_1^2+\Gamma_2^2\cdot\frac{(1-\Gamma_1^2)\cdot A^2\cdot(1-\Gamma_2^2)}{1-(A^2\cdot\Gamma_1\cdot\Gamma_2)^2}\right\}P_0. \qquad (2.3)
\end{aligned}$$

In the same way, the power reflected when sending a probe signal to port 2 is

$$P_{R_2}=\left\{\Gamma_2^2+\Gamma_1^2\cdot\frac{(1-\Gamma_2^2)\cdot A^2\cdot(1-\Gamma_1^2)}{1-(A^2\cdot\Gamma_2\cdot\Gamma_1)^2}\right\}P_0. \qquad (2.4)$$

As a result of Eq. (2.3) and Eq. (2.4), a passive component can have different reflection parameters $S_{11}\neq S_{22}$. Equations (2.2 - 2.4) allow one to calculate the reflection coefficients from the measured S-parameters of the SSPF.

$$\Gamma_1 = \sqrt{\frac{S_{11}^2 - S_{12}^2 S_{22}^2}{1 - S_{12}^4}} \tag{2.5}$$

$$\Gamma_2 = \sqrt{\frac{S_{22}^2 - S_{12}^2 S_{11}^2}{1 - S_{12}^4}} \tag{2.6}$$

Absorption by the filter is commonly described with the loss factor, which is defined via the relations

$$1 = |S_{21}|^2 + |S_{11}|^2 + FLF \tag{2.7}$$

$$1 = |S_{12}|^2 + |S_{22}|^2 + RLF \tag{2.8}$$

Here, FLF (RLF) is the forward (reverse) loss factor referring to a probe signal applied at port 1 (2). Since, as outlined above, in general $S_{11} \neq S_{22}$, FLF and RLF can also be different. An ideal filter should have no loss and no reflection in its passband, but in its stopband it is necessary that the transmission parameter is zero. Hence either the reflection parameter or the loss should be high in the stopband. If the reflection is high, reflected signals can distort the initial signal. In our SSPF reflective and absorptive filtering mechanisms coexist.

For complex DUT it is helpful to define a normalized loss factor with the transmitted power as reference. This normalization can be done by multiplying the FLF with $\frac{1}{1-|S_{11}|^2}$ and the RLF with $\frac{1}{1-|S_{22}|^2}$.

2.4 Spatially resolved impedance measurements

In a microwave setup impedance is a crucial quantity regarding reflections, which occur due to impedance mismatches. For this reason a method to study the impedance levels of SSPF in detail is described in the following.

2.4.1 Time-domain reflectometry (TDR) setup

Time domain reflectometry (TDR) is a technology to localize the impedance discontinuities in the DUT via their associated reflections. A TDR measurement setup is shown in Fig. 2.9.

The TDR sampler emits a step pulse V_1^+ with a rise time of a few picoseconds (equating a bandwidth of 30 GHz) and measures the reflected amplitudes V_1^- as a function of time. The result is converted into impedance data using the equations

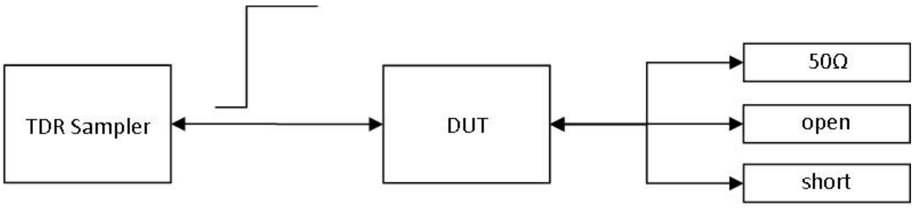

Figure 2.9: TDR setup for position-sensitive impedance measurements.

$$\Gamma = \frac{V_1^-}{V_1^+} = \frac{Z_L - Z_0}{Z_L + Z_0} \tag{2.9}$$

$$\text{and } Z_L = Z_0 \frac{1+\Gamma}{1-\Gamma}. \tag{2.10}$$

Here, Z_L is the impedance of DUT and $Z_0 = 50\,\Omega$ is the characteristic impedance. If there is an increase (decrease) of impedance in the DUT, the reflected pulse is in (180° out of) phase. Hence, an open circuit ($Z_L = \infty$, $\gamma = 1$) causes a full in-phase reflection and a short circuit ($Z_L = 0$, $\gamma = -1$) a full out-of-phase reflection. A $50\,\Omega$ termination ($Z_L = 50\,\Omega$, $\gamma = 0$) is a perfect match with zero reflection. Several examples of typical loads and their TDR data are presented in App. C.

Another important feature of the TDR setup is the ability to locate mismatches. When the propagation speed of the step pulse is known, the location of a reflection point can be derived from the time delay of the reflected signals. The bandwidth of the step pulse (30 GHz) defines the temporal and therefore the spatial resolution. A typical TDR trace is shown in Fig. 2.10.

TDR is complementary to S-parameter measurements described in Sec. 2.3. Whereas the latter gives access to the frequency dependence of reflections, TDR reveals the location of one or more reflection points inside the DUT.

2.4.2 Estimation of propagation speed

In order to attain the electrical length s_{el} from TDR, the propagation speed v_{med} in the relevant medium must be known. By connecting two Minibend cables of different lengths Δs to the TDR sampler and measuring the transit time Δt, the propagation speed

$$v_{\mathrm{med}} = \frac{\Delta t}{\Delta s} \tag{2.11}$$

can be estimated:

Cable	length Δs/mm	transit time Δt/ns	$v_{\mathrm{med}}/\frac{\mathrm{m}}{\mathrm{s}}$
Minibend - 10 0810	254	2.42	$1.05 \cdot 10^8$
Minibend - 5 0808	127	1.23	$1.03 \cdot 10^8$

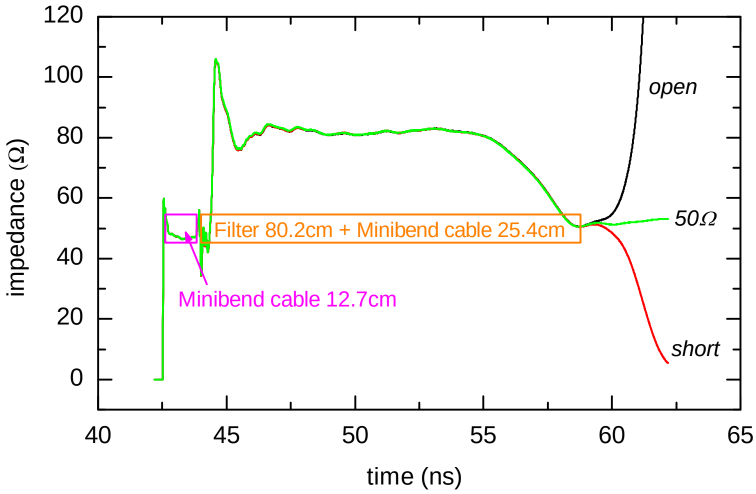

Figure 2.10: Typical TDR trace. Sudden impedance changes indicate reflection points such as connectors or mismatched components. Also, the signatures of a short circuit, a 50 Ω load and an open circuit are shown.

By averaging, we obtain an average propagation speed

$$\overline{v_{\mathrm{med}}} = 1.04 \cdot 10^8 \, \frac{\mathrm{m}}{\mathrm{s}} \approx 0.35 \cdot c_0 \tag{2.12}$$

for Minibend cables. Finally, we note that the propagation speed also allows one to convert frequency into wavelength:

$$\lambda = \frac{v_{\mathrm{med}}}{f} \approx 0.35 \frac{c_0}{f} \; . \tag{2.13}$$

2.5 Microwave simulations with ADS

Todays advanced microwave simulation software can help to significantly reduce the measurement time. For this thesis, ADS2009 (Advanced Design System) from Agilent is used [10]. To this end, all S-parameters of all SSPF are recorded and fed into the software. In ADS, the filter then acts as an arbitrary device with defined S-parameters, which can be combined with various matching circuits from the ADS library. For arranging the components of the setup, the interface of ADS is designed like a large pinboard, where devices can be placed and connected with ideal wires (cf. Fig. 2.11). In a transient measurement, a square pulse is sent through the simulated setup and read out at the end.

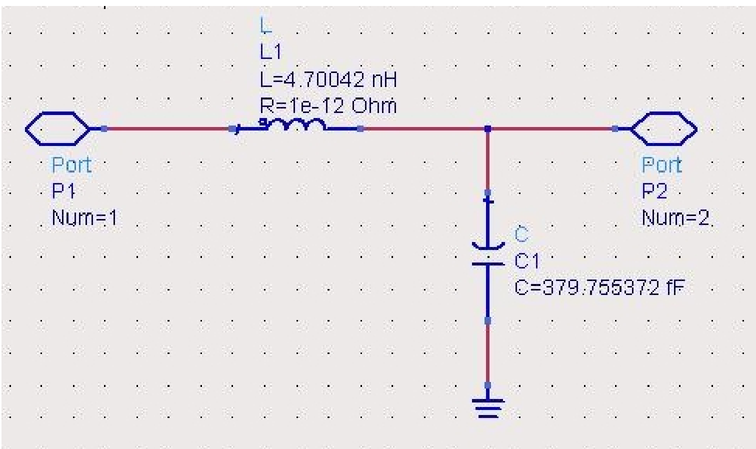

Figure 2.11: A simple matching circuit in ADS with a coil and a capacitor.

Chapter 3

Analysis of non-impedance matched stainless steel powder filters

In order to find strategies for impedance matching, the standard SSPF designs have to be characterized thoroughly. In this chapter, we present the results of S-parameter, TDR, and pulse transmission measurements (for details on the setups cf. Ch. 2).

For both asymmetric and symmetric filter design, the wire length and the number of windings per unit length are varied. All other parameters such as the powder material, grain size, the wire or casing material and diameter were kept constant. They are summarized in Table 3.1.

powder		wire		casing	
material	grain size	material	diameter	material	inner diameter
stainless steel	325 mesh = 44 µm	copper	200 µm	copper	5.10 mm

Table 3.1: Parameters of SSPF

Within the scope of this thesis, all measurements and optimizations are performed at room temperature. Phenomena specific to cooled filters [1] are not considered. Nevertheless, our results are also highly relevant for SSPF operated in cryogenic environments.

3.1 Pulse transmission

In many experiments on superconducting flux quantum circuits [11], microwave or quasi-DC voltage pulses are required. In particular, the rise times of the edges in the pulse envelope are on the nanosecond or even subnansecond timescale. Such sharp pulse edges involve high-frequency components, which are attenuated by SSPF. Hence, an optimum between filter attenuation and accurate pulse shape has to be found.

The test pulse for our SSPF has a typical sample-and-hold configuration widely used in experiments on superconducting flux qubits [11]. It consist of a 50 ns square "sample" pulse, which for technical reasons is followed by a 1 µs "hold" stage. As shown in Fig. 3.1, the destructive effects of poorly impedance matched SSPF is most evident in and near

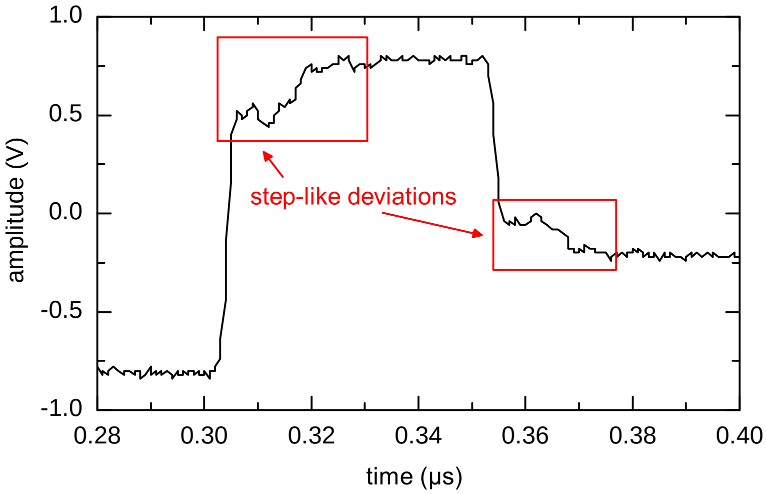

Figure 3.1: Sample-and-hold pulse showing step-like deviations caused by a non-impedance matched SSPF.

the ”sample” pulse. In this situation, the SSPF produces step-like deviations, which are caused by a backward-reflection from the connector at the end of the filter followed by a forward-reflection from the connector at the beginning of the filter. Hence, the reflected signal passes the filter twice as shown in Fig. 3.2). Additionally, parts of the signal are already reflected by the first connector without entering the filter and do not reach the oscilloscope at all.

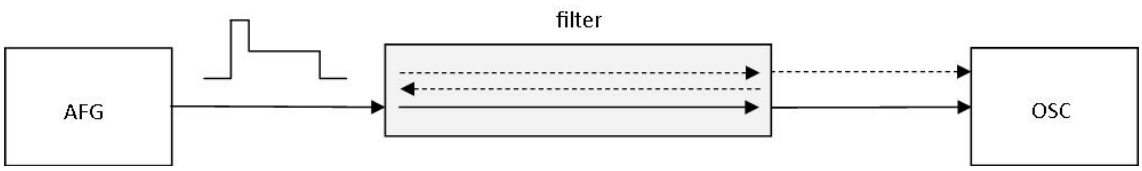

Figure 3.2: Diagram of pulse reflection inside a filter.

The doubly reflected signal has a smaller amplitude than the directly transmitted one and reaches the oscilloscope with a delay of

$$\Delta t_{\text{calc}} = \frac{2\Delta s_{\text{wire}}}{v_{\text{med}}} \tag{3.1}$$

where Δs_{wire} is the length of the copper wire inside a SSPF and v_{med} the velocity in a medium. As illustrated in Fig. 3.3, this results in a characteristic pulse form with a step. The comparison of the pulse distortions caused by SSPF with various lengths shown in Fig. 3.4 indeed shows that the width of the step scales with the length of the wire inside the filter. Furthermore, as expected, the maximum transmission amplitude decreases with longer SSPF wire.

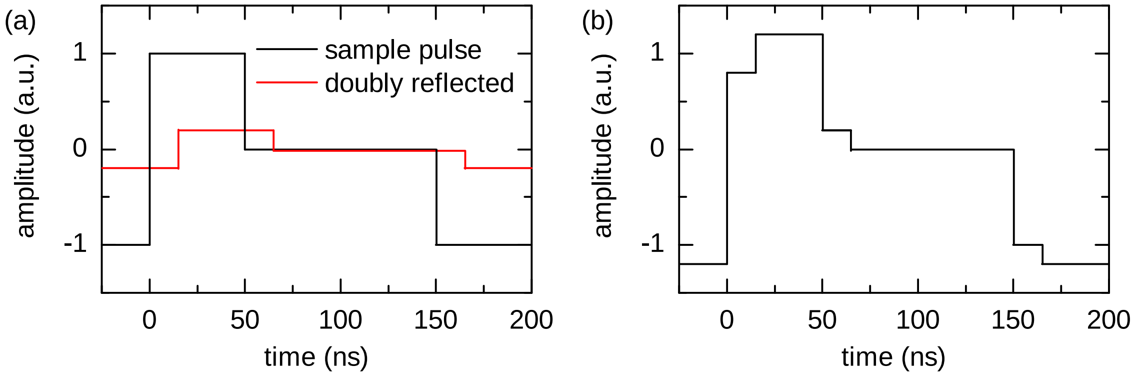

Figure 3.3: Reflection of a sample pulse: In (a) the red graph denotes a doubly reflected and attenuated reflection of the initial pulse (black). (b) shows the superposition of the initial pulse and the first reflected pulse.

In this context, we note that filter SSPF 97.3 cm constitutes an exception. It has an unusually low transmission hindering a precise determination of the step position. It is because this filter has a short circuit between the inner wire and the copper casing, which will be revealed by a TDR spectroscopy later on.

Moreover it is seen in Fig. 3.4 that the step of SSPF 157.4 cm is larger, since the values of the reflection parameters, S_{11} and S_{22}, of this filter are higher than usual due to the irregular winding of its core.

3.1.1 Linear relation between step length and wire length

For the length of the step we get the following time differences as far as the beginning and end of the step was identifiable:

wire length $\Delta s_{\text{wire}}/\text{cm}$	step length $\Delta t_{\text{meas}}/\text{ns}$	$\Delta t_{\text{calc}}/\text{ns}$	$\frac{2\Delta s_{\text{wire}}}{\Delta t_{\text{meas}}} \;/\; \frac{\text{cm}}{\text{ns}}$
157.4	26.6	30.0	11.84
106.6	15.0	20.3	14.22
105.9	16.0	20.2	13.24
97.3	short circuit		
96.5	14.0	18.4	13.78
80.2	12.9	15.3	12.44
79.5	13.1	15.2	12.14
57.3	7.3	10.9	15.70

Even if the step lengths differ when looking at a pair of similar filters, for instance SSPF 80.2 cm and SSPF 79.5 cm, one can see clearly the tendency of the step length becoming smaller when the wire length decreases. As shown in Fig. 3.5, this relation is

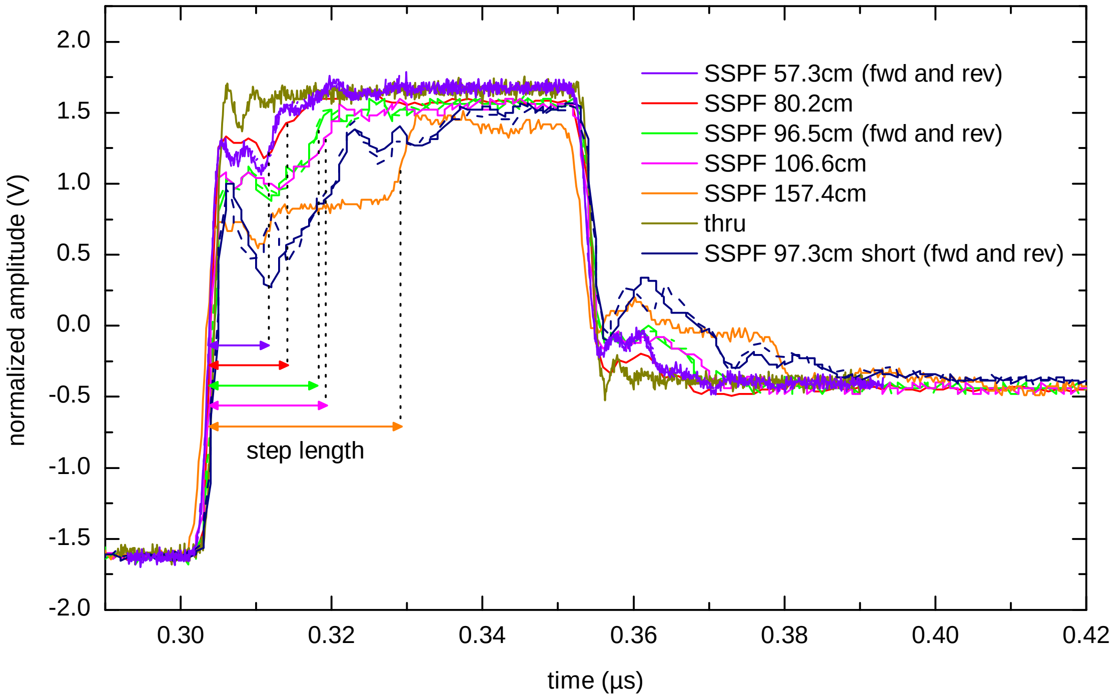

Figure 3.4: Normalized pulse transmission of asymmetric SSPF. Different wire lengths result in steps of different lengths (positions are indicated with arrows).As discussed in Sec. 2.3.2, the orientation of the SSPF only affects the transmitted signal weakly (solid lines: Port 1 of the filter at AFG, dashed lines: Port 2 at AFG). For technical reasons, thru, SSPF 57.3 cm, SSPF 80.2 cm and SSPF 157.4 cm, are recorded with an initial pulse amplitude of 10 V plus a 10 dB attenuator, while the others are recorded with an initial pulse amplitude of 4 V plus a 2 dB attenuator.

approximately linear (Pearson R value[1] of 0.982). Surprisingly, the propagation speed inside the SSPF is very similar to the propagation speed of 0.35c inside the Minibend coaxial cables measured with TDR in Sec. 2.4.2.

3.2 Filter attenuation

In this section we discuss the attenuation properties of the SSPF in the frequency domain by measuring their S-parameters as described in Sec. 2.3.1.

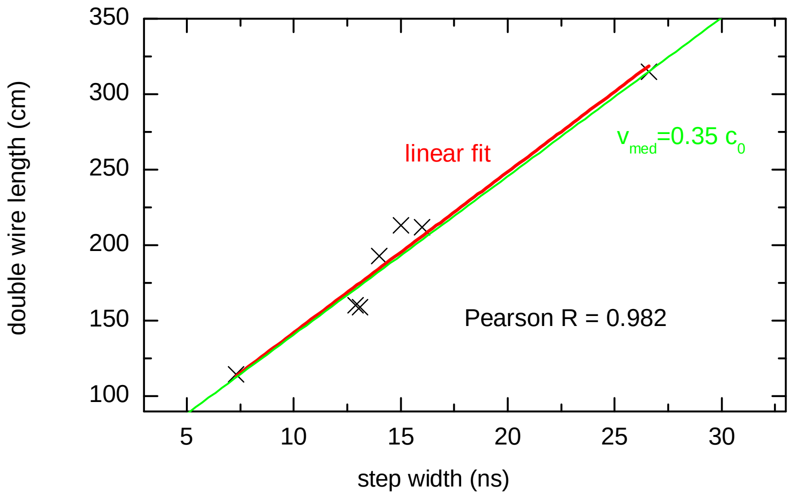

Figure 3.5: Linear scaling of wire length and width of reflected step: When plotting two times the wire length Δs_{wire} against the step width Δt_{meas}, which can be extracted from Fig. 3.4, the slope describes the propagation speed in a medium v_{med}. Black crosses: data. Red line: linear fit to data. Green line: propagation speed inside the Minibend coaxial cable measured in Sec. 2.4.2.

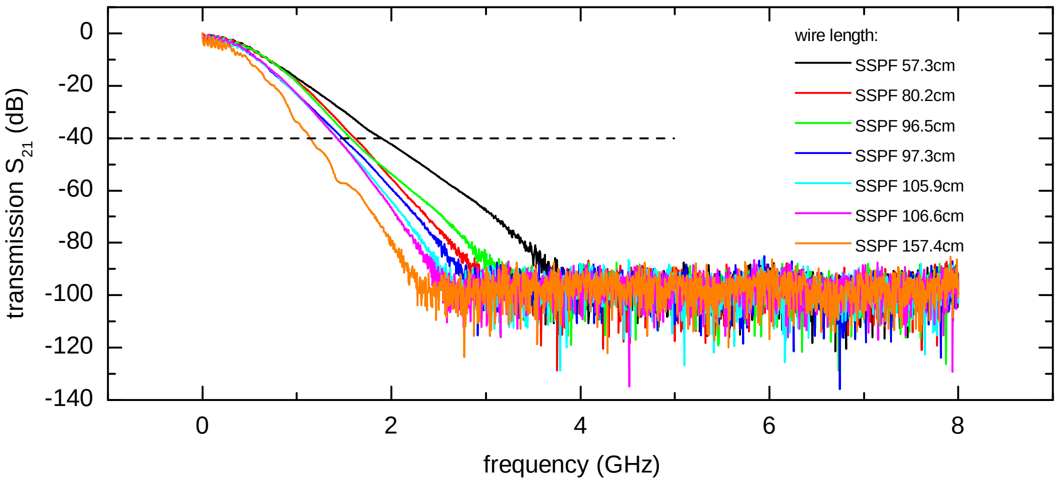

Figure 3.6: Attenuation characteristics of asymmetric SSPF with wire lengths between 57.3 cm and 157.4 cm. The dashed line denotes an attenuation of 40 dB.

3.2.1 Asymmetric SSPF

The total attenuation of the SSPF (absorptive and reflective) is obtained from measurements of the transmission parameters S_{21} (forward) and S_{12} (reverse). Since SSPF are passive devices ($S_{21} = S_{12}$), we restrict ourselves to forward transmission measurements.

[1]Pearson R is a quantity for linearity. It has values between -1 and 1, which corresponds to a positive or negative linear correlation. If the Pearson R is 0, then no linearity exists [12].

The results are plotted in Fig. 3.6. The transmission signal falls below the noise floor of the network analyzer between 2 and 4 GHz and stays there up to at least 40 GHz. As a general trend, filters with longer wire have a steeper characteristics. More specifically, the frequency of 40 dB attenuation is found to depend linearly (Pearson R value of -0.974) on the wire length as shown in Fig. 3.7.

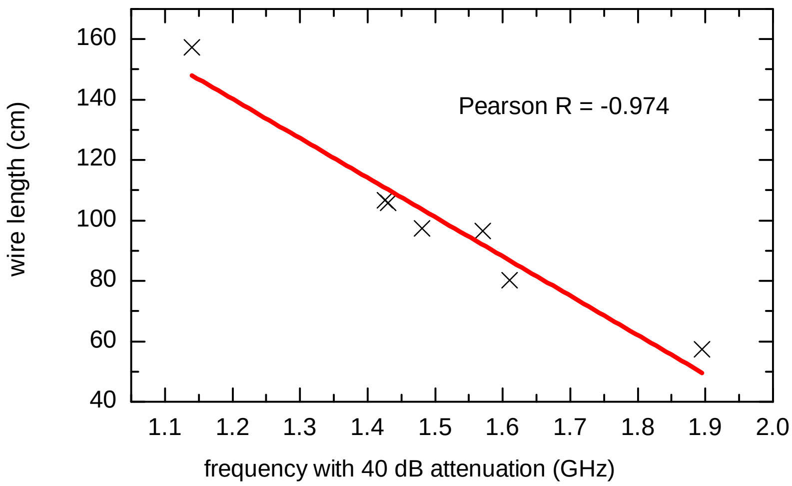

Figure 3.7: Frequency with attenuation of 40 dB the frequencies of the SSPF as a function of the wire length. Crosses: data. Red line: linear fit.

Additionally, Fig. 3.6 reveals that the details of the attenuation characteristics are sensitive to the geometric layout of the SSPF. In particular, the SSPF with 80.2 cm wire length shows an unusually steep characteristics because its wire is wound around the core with a pitch of 1 mm instead of 0.75 mm for all other filters. Furthermore, the characteristics of the SSPF with 157.4 cm wire length exhibits wiggles which are due to the fact that the pitch of the copper wire is not homogeneous enough. Nevertheless, the influence of the pitch on the filter attenuation is rather minor.

3.2.2 Reflection parameters

Access to the reflection and absorption coefficients can be gained by measuring the reflection parameters S_{11} and S_{22} in addition to the transmission. A prototypical result is shown in Fig. 3.8. As pointed out in Sec. 2.3.2, the determination of the exact reflection and absorption coefficients requires knowledge of the internal device structure. However, useful qualitative insight can already be gained from S_{11} and S_{22} directly.

We first note that S_{11} differs strongly from S_{22} as expected for an asymmetric SSPF. Furthermore the reflection depends strongly on frequency and reaches up to -3.98 dB (0.63 power ratio) in the passband, explaining the step in the square pulse (cf. Fig. 3.1). We finally note that even for frequencies well above the passband, where the transmission is already below the noise floor of the VNA, the filter behavior does not only depend

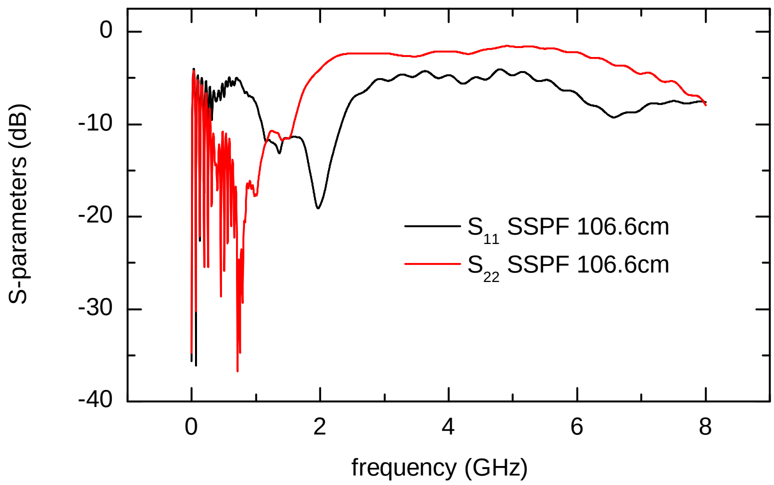

Figure 3.8: Reflection parameters S_{11} and S_{22} the asymmetric SSPF with 106.6 cm wire length.

on absorption, but also significantly on reflection. Regarding the filter asymmetry, TDR spectroscopy will give a more detailed insight (cf. Sec. 3.3).

3.2.3 S-parameters of symmetric filters

The symmetric filters with Teflon or Kapton closing show an attenuation behavior similar to that of the asymmetric filters, reaching the noise floor at about 3 GHz (cf. Fig. 3.9). At low frequencies the reflection ratio is less than -4 dB (0.40 power ratio) providing a good transmittance. In the stopband of the filter the reflections are comparable to those of asymmetric filters. As expected from the more symmetric mounting procedure of the connectors, reflections in both directions (S_{11} and S_{22}) show a similar magnitude and frequency dependence.

However, we note that the symmetric SSPF with Kapton closing tend to have a reduced attenuation at frequencies above a few gigahertz. This problem, which is shown in Fig. 3.10, remains to be addressed in future work.

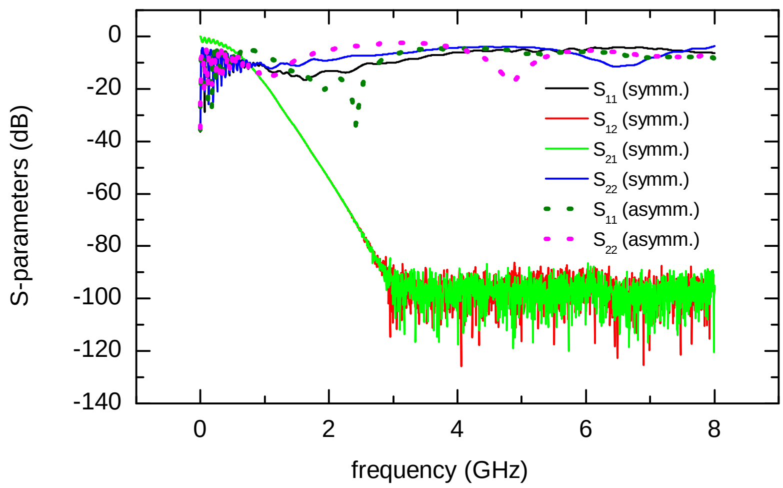

Figure 3.9: S-parameters of a symmetric filter with Teflon closing (SYM-SSPF 94.5 cm-T) compared to S-parameters of an asymmetric filter with SMA connectors (SSPF 105.9 cm): The reflection parameters S_{11} and S_{22} look more similar for symmetric filters.

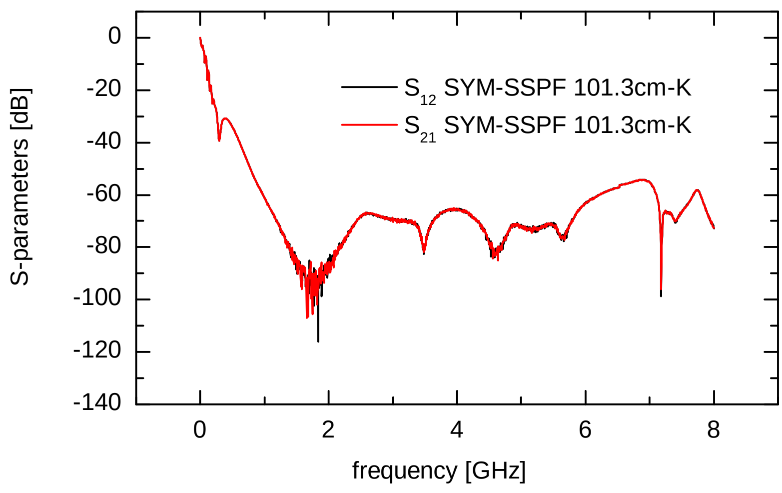

Figure 3.10: S-parameters of a symmetric filter with Kapton closing (SYM-SSPF 101.3cm-K) with a reduced attenuation at higher frequencies.

3.2.4 Filters without stainless steel powder

In order to examine the effect of the stainless steel powder on the filter attenuation, we fabricate filters with massive metal cores (copper, stainless steel or gold plated copper) and no powder inside a standard copper casing. Looking at Fig. 3.11, it is obvious that these filters without powder have only little attenuation. The origin of this remaining attenuation may be found in the resistance of the wire and in the coil, which functions as an antenna and radiates power. We find the attenuation characteristics of the filters with massive metal cores and no powder to be independent of the core material. Other powder materials, however, result in a different filter quality [2].

The blue graph in Fig. 3.11 is a filter with a core in ∞-form made of a Stycast and stainless steel powder mixture, but without powder filling as well. It shows a considerable attenuation but the fall-off is not as steep as that of a filter filled with powder, even if the wire length is the same.

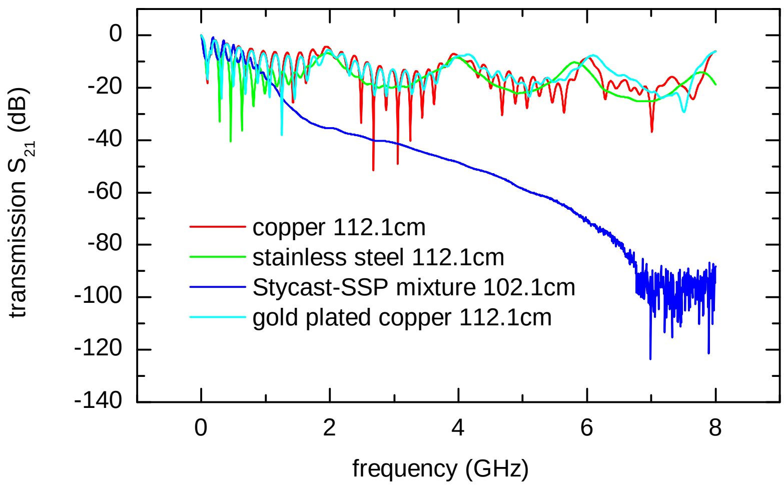

Figure 3.11: Attenuation for different core materials: Filter with core made of Stycast and stainless steel powder mixture (102.1 cm wire length), copper, gold plated copper and stainless steel (each 112.1 cm). All cores have a pitch of 0.75 mm.

Hence we conclude that it is indeed the metal powder which causes most of the attenuation. To achieve a high powder density, we use the vibrating apparatus as described in App. A.

3.2.5 Loss factor

The absorptive behavior of the SSPF can be understood by analyzing the forward, reverse, and normalized loss factors introduced in Sec. 2.3.2. In Fig. 3.12(a), FLF and RLF are plotted for asymmetric SSPF. As expected for a lowpass filter, the loss factor increases steeply with the steepness of the frequency fall-off depending on the wire length. At higher frequencies, the loss factor remains on a high level although the details of FLF and RLF differ due to the asymmetry between S_{11} and S_{22}.

Figure 3.12(b) shows that the symmetric SSPF exhibit significantly less difference between FLF and RLF as expected from their more symmetric reflection properties. At high frequencies, the symmetric SSPF with Teflon closing have a higher loss factor than those with Kapton closing. Since the difference in attenuation of otherwise identical filters should be negligible, we conclude that the Teflon closing causes more reflections and, hence a larger mismatch. This conclusion is confirmed by TDR measurements in Sec. 3.3.3.

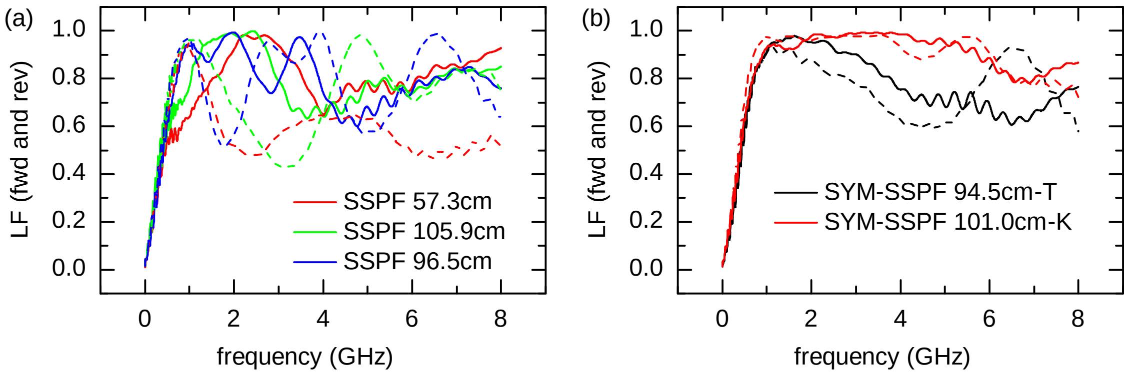

Figure 3.12: Loss factor for (a) asymmetric, (b) symmetric filters. The solid lines denote the FLF and the dashed lines the RLF.

The pure absorption behavior of the filters is better seen in the normalized loss factors shown in Fig. 3.13. It shows a steep increase at low frequency and remains constantly close to unity thereafter. The dummy filter without metal powder clearly shows an inferior performance as expected from the transmission measurements shown in Fig. 3.11. Filters with metal powder only in the core do show some attenuation, but less than filters which are completely filled with metal powder. These results confirm that the filter attenuation is mainly caused by the metal powder.

As a final remark, we note that the massive metal core in the dummy filters needs to be isolated from the wire with GE Varnish to prevent short circuits.

3.2.6 Step height and reflection parameters

Not only the width of the step is important in the analysis of the filters but also its height. The ratio between the height of the step and the amplitude of the pulse is the average reflection coefficient S_{11} or S_{22} [cf. Eq. (2.1)]. At this point we restrict ourselves to the example of a symmetric filter, because its S_{11} and S_{22} do not differ much. The height of the step from the filter with Kapton closing (SYM-SSPF 104.0cm-K) is about 0.129 times the total amplitude of the pulse [cf. Fig. 3.14(a)]. So the calculated reflection parameter

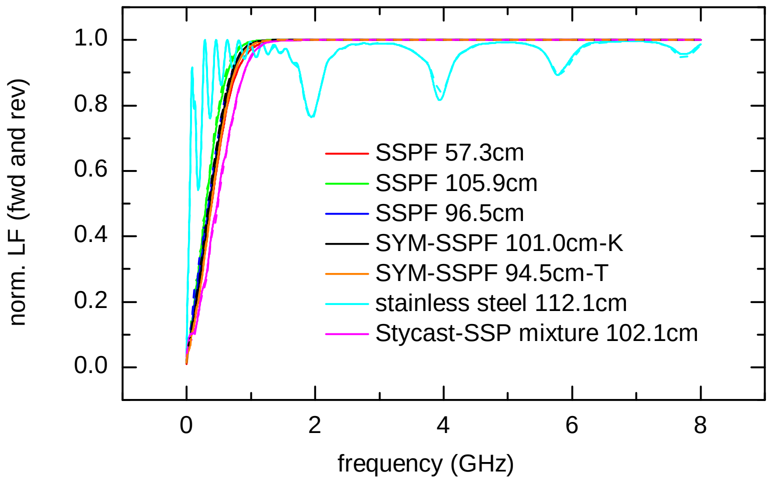

Figure 3.13: Normalized loss factor for different DUT: A core made of massive stainless steel has a worse power absorption than a core made of a Stycast stainless steel powder mixture. Hence metal powder is the absorptive part of the filter.

is 0.144, which equates -16.8 dB. This calculated value fits well into the S-parameters diagram of this particular filter [cf. Fig. 3.14(b)].

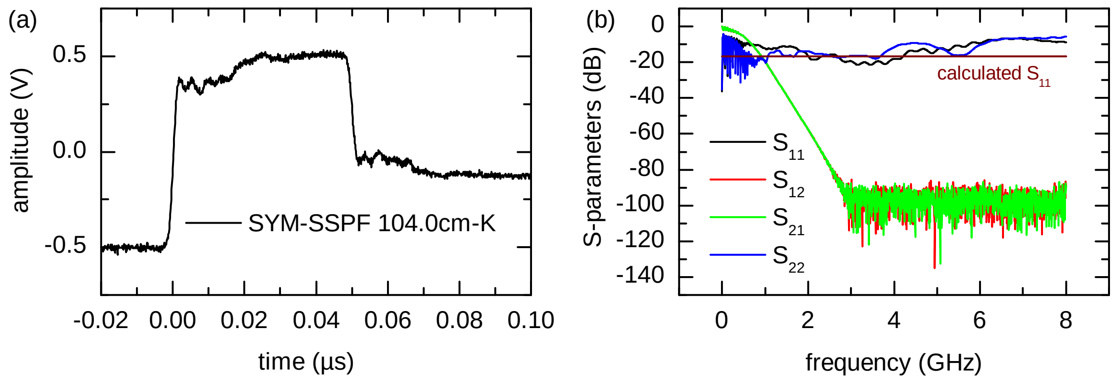

Figure 3.14: (a) Pulse transmittance of a symmetric filter with Kapton closing (wire length 104 cm). (b) S-parameters of the same symmetric filter and calculated reflection coefficient S_{11}.

3.3 Impedance

The reflections seen in the pulse transmission measurements (Sec. 3.1) and confirmed by S-parameter measurements (Sec. 3.2) indicate a severe mismatch between the SSPF and their 50 Ω load impedance. In order to determine the spatial location of this mismatch, we perform TDR spectroscopy. In this way, we also obtain information on the impedance inside the SSPF. The TDR data, which is not frequency resolved, is complementary to the frequency resolved S-parameter measurements.

3.3.1 Impedance of asymmetric SSPF

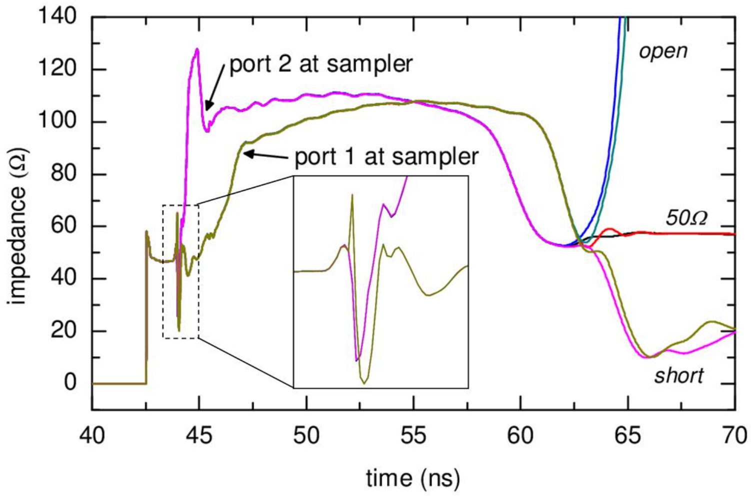

Figure 3.15: Impedance levels for an asymmetric filter (SSPF 106.6 cm). The blowup shows the characteristic notch at the beginning of the filter.

Figure 3.15 shows the TDR signal of an asymmetric SSPF (SSPF 106.6cm), measured from both directions. This graph is a characteristic example for all asymmetric SSPF fabricated during this thesis. Port 1 is the port, which is first put into the copper casing during the fabrication process. After the filling process port 2 was used to close the filter. Therefore the wire between port 2 and the core is longer than the wire between port 1 and the core (cf. Sec. 2.1.1). Moreover the routing of the wire at port 2 is not well defined. The result of this fabrication process can clearly be seen in Fig. 3.15. The first feature on the left is the TDR step, followed by the 50 Ω Minibend cable. Next, there is a narrow impedance notch down to 20 Ω for both measuring directions. Connected with port 1 at the sampler the impedance increases smoothly up to 105 Ω, whereas the port-2-graph shows a high peak up to 130 Ω and then reaches a level of 110 Ω. In both cases, the impedance falls back to approximately 50 Ω at the end of the filter and then shows the expected behavior depending on the termination method (open, 50 Ω, short).

We conclude that it is necessary to keep the wire between the connector and the first winding of the core short, otherwise a high peak in impedance is measurable causing the reflection parameter S_{22} being higher than S_{11} (cf. Fig. 3.8).

3.3.2 Pitch of the core and impedance level

Since the pitch of the core, i.e., the density of windings, is expected to be a crucial parameter for the attenuation performance, filters with different pitches were measured. From Fig. 3.16 we know that the overall impedance level does not depend on the length of the filter but on the pitch of the core. SSPF 80.2 cm and SSPF 79.5 cm have a pitch of 1 mm, whereas the others have one of 0.75 mm, which results in an impedance of 80 Ω and 90-108 Ω respectively. The closer one winding is to the next, the higher the impedance, a behavior consistent with the properties of a standard magnetic coil.

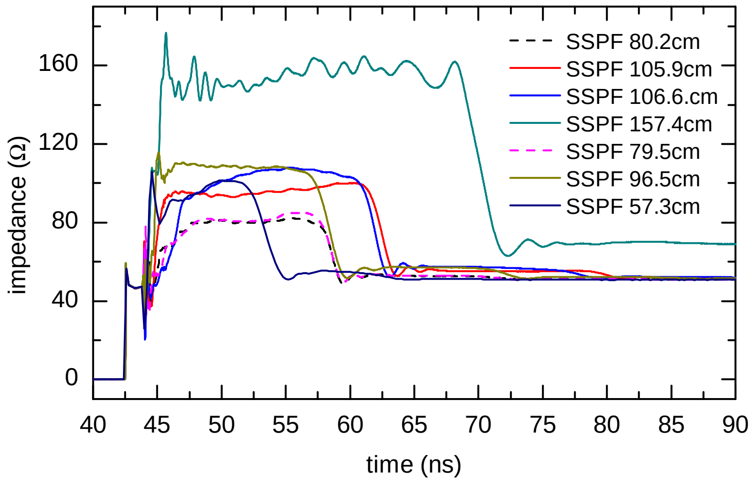

Figure 3.16: Impedance levels of filters with different core pitches: SSPF 80.2 cm and SSPF 79.5 cm have a core pitch of 1 mm (dashed graphs), whereas the other SSPF a pitch of 0.75 mm (solid graphs). The smaller the core pitch the higher the resulting impedance level. SSPF 157.4 cm has an exceptionally high impedance because of its inaccurate winding.

In this qualitative picture, the ∞-shape of our "coil" is not relevant. Furthermore, since the coil is no punctiform element, the impedance rises over some length from its initial level of 50 Ω to its overall impedance level. In the same manner it falls back to 50 Ω at the end of the coil.

Another important parameter is the accuracy of the winding. For instance the impedance of SSPF 157.4 cm is very high, because its core is wound inaccurately. As a result the impedance mismatch is quite large and therefore the step in the pulse transmittance is more pronounced.

3.3.3 Impedance level of symmetric filters

A first step towards impedance matched SSPF is to fabricate symmetric filters. For a detailed fabrication instruction see App. A. In this way, the transition between cable/connector and filter can be designed in a more controlled way. Looking at the TDR results for the symmetric filters fabricated in this work, we find that the first windings of the core are critical regarding impedance. Filters with Teflon or a foil of Kapton as closing have a controlled routing of the wire and are approximately symmetric. This can be seen very clearly in Fig. 3.17. In agreement with their pitch, also the symmetric filters exhibit an impedance of approximately $100\,\Omega$. Regarding the Teflon filter a slight slope is visible, whereas the impedance of the filter with Kapton closing remains constant. A reason for that might be a slightly irregular winding of the Teflon filter's core or the core lying tilted inside the copper casing, so that the wire is not equally shielded by powder. The magnified part shows the details due to the SMA connector and a printed circuit board used to connect the filter wire and the SMA connector. These features are discussed later in App. B.4.3. The symmetric filters are already a slight improvement over the asymmetric ones because the impedance peak at port 2 of the asymmetric filter (cf. Fig. 3.16) has disappeared.

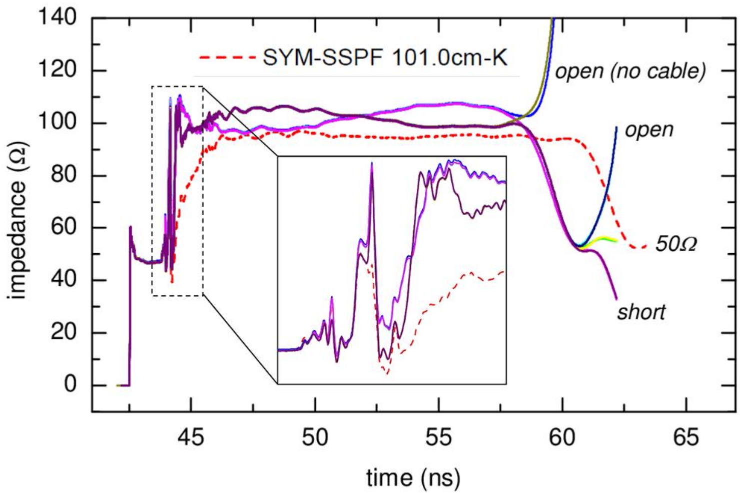

Figure 3.17: Impedance levels for symmetric filters: Solid lines are from a SSPF with Teflon closing, whereas the dotted line from a SSPF with Kapton closing. The two ports (violet and magenta solid line) behave similarly. The "open (no cable)" graphs have their origin in leaving out the Minibend cable after the SSPF. The blowup shows details due to the connection between filter wire and SMA connector.

3.3.4 Using TDR spectroscopy to identify short circuits

An additional feature of the TDR spectroscopy is to identify and locate short circuits in a filter. In this thesis one filter was spoiled during fabrication process and thus shows an abnormal impedance characteristic. From Fig. 3.18 it is obvious that the short circuit is at port 1, because when connecting the filter with its port 2 to the sampler, the characteristic remains normal until the TDR signal reaches port 1. There the impedance drops as if a short-cap was connected. In the port-1-direction the filter shows the same characteristics as a short-cap.

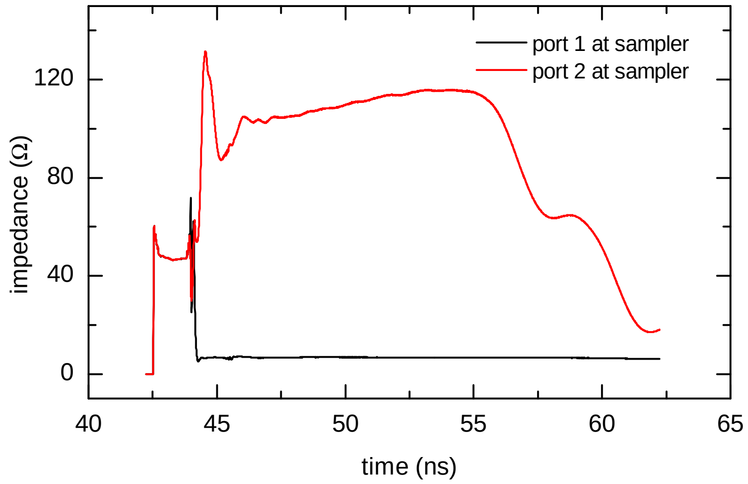

Figure 3.18: Impedance of SSPF 97.3 cm with a short circuit near port 1.

3.3.5 Frequency dependent impedance

Using the reflection data from the S-parameter measurements and Eq. (2.10) it is possible to calculate a frequency dependent impedance. The result is plotted in Fig. 3.19(a) and (b) for the asymmetric filters and in Fig. 3.19(c) for the symmetric filters. As expected, the graphs based on forward and reverse S-parameters differ strongly for asymmetric filters. Surprisingly, however, even for the symmetric Kapton and Teflon filters the forward and reverse impedance look clearly different. Our conclusion is that the frequency dependent impedance is very sensitive to small aberrations in the fabrication process. All the graphs show a high impedance in the stopband of the filter explaining the reflective part of the filter behavior. In the passband a definite analysis is not possible, because the data is mixed with measurement artifacts (high and narrow oscillations between 0 and 1 GHz). In agreement with the TDR measurements we find that SSPF 80.2 cm, which is the only filter with a core pitch of 1 mm, has an overall lower impedance. Also in the frequency-dependent impedance data we find that the symmetric configuration constitutes an improvement over the asymmetric configuration. In Fig. 3.19(c) we see that the frequency dependent impedance generally has the same maximum value for both directions, which is much lower than the maximum reverse impedance of the asymmetric SSPF.

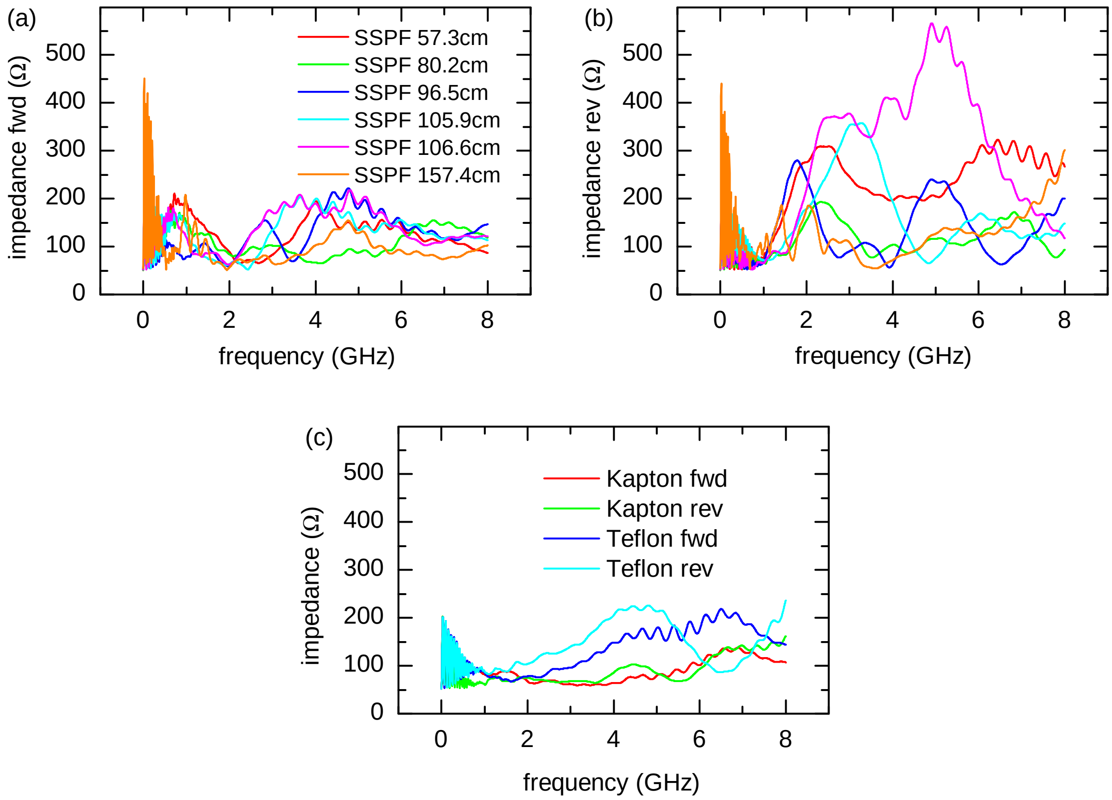

Figure 3.19: Frequency dependent impedance of SSPF: (a) forward and (b) reverse impedance, corresponding to S_{11} and S_{22}. For a (c) symmetric filter with Kapton or Teflon closing, both directions are nearly the same.

Chapter 4

Impedance matching of stainless steel powder filters

Having thoroughly analyzed the transmission and reflection properties of SSPF, we now turn to the discussion how to match these devices to a $50\,\Omega$ impedance. To this end, we first discuss the difficulties of an approach based on external matching circuits. Next, inspired by simulations, we present a simple and effective matching technique based on a parallel circuit of two SSPF with suitable geometry.

4.1 External matching circuits

In today's microwave technology, matching circuits are standard tools for reducing unwanted reflections, when two components of different impedance have to be connected. In the context of this work, the SSPF with their impedance of 80-100 Ω have to be matched to the $50\,\Omega$ standard of the connectors, cables, and other components. As discussed in Ch. 3, the mismatch is located between the connector and the wire wound around the filter core. However, the TDR signal is complicated in the transition region, making it difficult to determine the precise location of the mismatch. Hence, the first idea is to "pull" the mismatch out of the filter by inserting a short suitable printed circuit board (PCB) between connector and copper wire. Then, at a later stage, the mismatch can be treated with a suitable matching circuit on this PCB.

We investigate three PCB layouts: with microstrip transmission lines, with coplanar wave guide transmission lines, and with lumped-element T-attenuators. For each layout, various designs are tested and optimized The details regarding design and analysis of those structures can be found in App. B.

In summary, even though it is possible to demonstrate an impedance transition on the PCB, there is still a mismatch inside the filter as shown in Fig. 4.1.

In Fig. 4.1 one can see the various effects for the example of a symmetric SSPF with Teflon closing and microstrip PCBs. After the board there is a high peak caused by a small part of wire ($l \approx 2\,\mathrm{mm}$) in the Teflon closing. Thin wire surrounded by Teflon, which has a low dielectric constant $\epsilon_{r,\mathrm{Teflon}} \approx 2$, results in a high impedance, because it

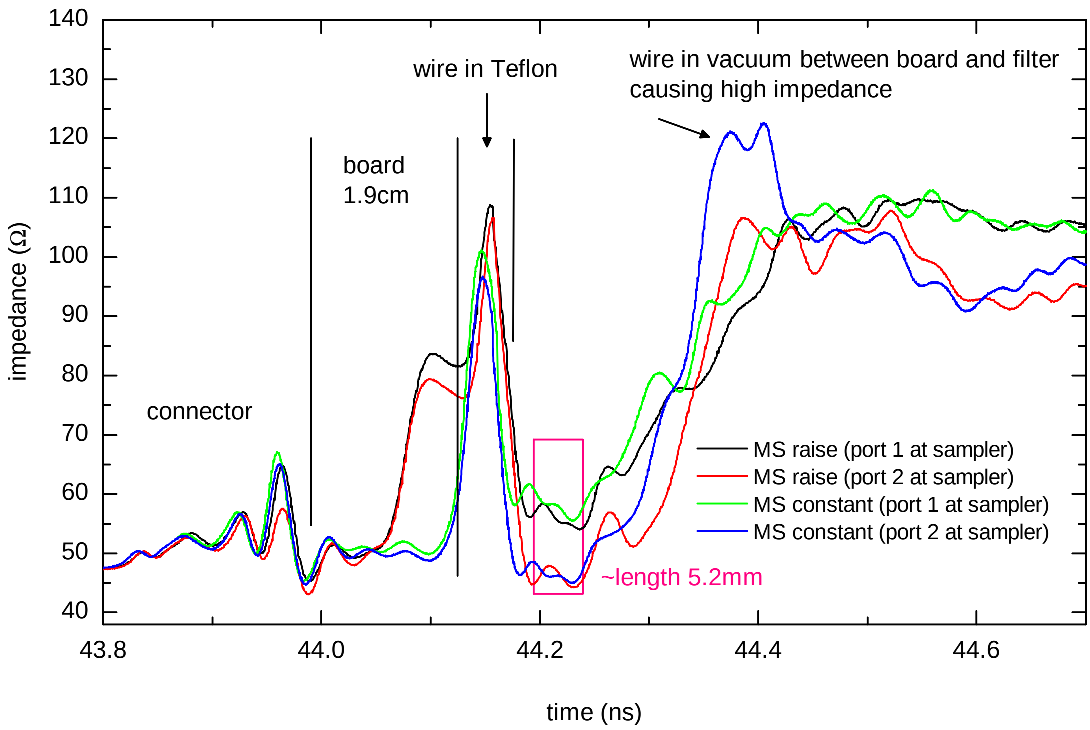

Figure 4.1: TDR data of a symmetric SSPF with Teflon closing and microstrip (MS) PCBs: Two different configurations, one with an impedance raise from 50 Ω to 80 Ω and one with a constant impedance of 50 Ω are compared.

acts like a cylindric capacitor with low capacitance

$$C = 2\pi\epsilon_0\epsilon_r \frac{l}{\ln\frac{r_{\text{casing}}}{r_{\text{wire}}}} \,. \tag{4.1}$$

Furthermore the ratio of the copper casing's inner radius r_{casing} and the radius of the thin wire r_{wire} is high, diminishing the capacitance even more. As the impedance of a transmission line is proportional to $\sqrt{\frac{1}{C}}$, a peak in impedance is the result.

Interestingly, after this peak the impedance drops to 50 Ω or 60 Ω respectively for a length of about 5.2 mm. The reason is that the core of the filter behaves like a magnetic coil with impedance caused by inductance, resistance and capacitance. Edge effects at the beginning of the coil lead to an impedance rise, because the first few windings are not completely covered with stainless steel powder and are less subjected to the influence of the other windings. At the beginning of the coil the inductance is relatively small and therefore the impedance is low. Only an ideal coil without edge effects would have a constant impedance required for the application of an external matching circuit.

As a result impedance matching of the SSPF based on using external structures is not possible without extensive changes in the design of the filter (e.g., powder material, core geometry, casing geometry, etc.). In order to avoid tedious trial and error, we continue with a simulation of the whole setup, where other methods can be tested easily.

4.2 ADS simulations on matching techniques

In order to get a quick overview over the possibilities how to match a filter's impedance, the S-parameters of the SSPF were put into the simulation software ADS2009 (Advanced Design System, cf. Sec. 2.5) from Agilent and different setups are investigated. Similarly to the experimental results presented above, no synthesized matching circuit could minimize the reflections.

Hence, since we know that external matching circuits are not helpful to minimize reflections, a new path has to be chosen. The key idea is that the overall impedance of a SSPF with a pitch of 0.75 mm is approximately 100 Ω, neglecting edge effects (cf. Fig. 3.16). Consequently, connecting two similar filters in a parallel circuit should result in an overall impedance of 50 Ω. Indeed the simulation shows, that a parallel circuit has significantly less reflection than a single filter (cf. Fig. 4.2)

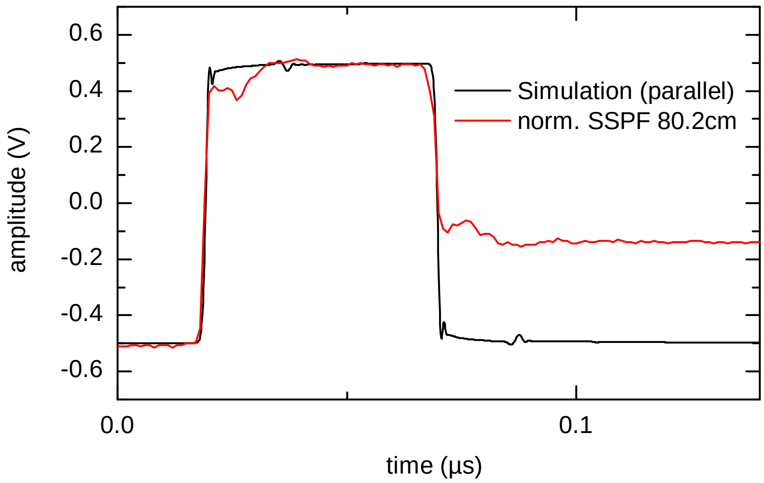

Figure 4.2: Simulation of transmitted pulse through parallel circuit of two filters with Kapton closing connected with two simulated PCB with a rectangular-mitered T-junction (cf. Fig. 4.3) and measurement of SSPF 80.2cm. Note that the simulation is performed with a purely rectangular pulse without hold level.

For a realistic simulation of setups with symmetric filters, in principle microstrip PCB with a T-junction have to be included. However, we find that the design of the T-junction does not affect the pulse transmittance (cf. Fig. 4.4). Hence, we omit the boards in most simulations.

In the following we present a summary of the key results of the ADS simulations on impedance matching of SSPF using a parallel circuit configuration.

- With our typical fabrication parameters, reflections are minimized when using two identical filters in parallel.
- More than two filters cause more reflections because the overall impedance is not 50Ω anymore.
- Using one filter with 80 cm and one with 105 cm length in parallel results in a worse pulse transmission than for two parallel 80 cm filters. The 80 cm filters have an overall impedance of $80\,\Omega$ and the 105 cm filters have $100\,\Omega$. From this point of view, the combination of two 80 cm filters should be worse than the combination of one 80 cm and one 105 cm filter, because the impedance mismatch would be larger. As a result it is the difference in the length, which causes the distortion, because the split signal is not recombined properly afterwards.
- If one branch of the parallel circuit is extended with a longer cable of 50Ω impedance, the reflections increase.
- Once the filters are connected in parallel and an overall impedance of about 50Ω is achieved, none of the synthesized matching circuits resulted in further improvement.

Additionally there are more effects with real components:

- Putting the filters first to the AFG and then connecting two identical cables makes the pulse look a bit clearer than putting the filters after the cables. This indicates a small effect of initial reflections.
- When using almost symmetric filers with Kapton closing, turning one filter around inside the sample holder and connecting it reversely does not affect the pulse much.
- Turning the whole sample holder around and connecting it with its port 2 at the AFG does not show any difference.

From these observations one can deduce three simple design rules for impedance matched SSPF:

1. The overall impedance has to be approximately $50\,\Omega$.
2. The lengths of the branches have to be equal.
3. Initial reflections at the filter entrance should be taken care of in the setup, e.g., with attenuators.

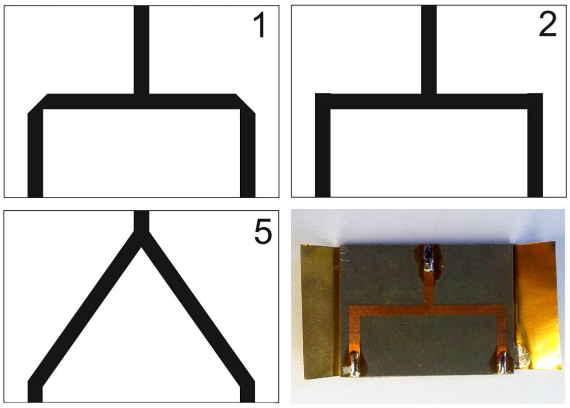

Figure 4.3: Microstrip T-junction design patterns: Black parts are conductive. All strips have an impedance of 50 Ω. The designs are 90° with mitered edges (1), 90° plain (2) and 60° plain (5). Photograph: actual sample. A brass sheet soldered to the back of the PCB provides a well defined ground plane.

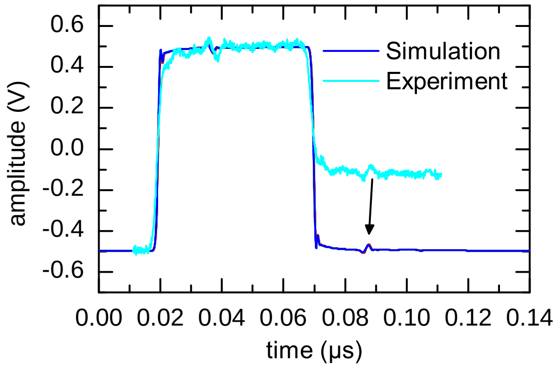

Figure 4.4: Comparison between simulation and real experiment: All simulations with different microstrip T-junction boards have exactly the same graphs and are in excellent agreement with the measurement. Black arrow: Even small features coincide between simulation and experiment. Note that the simulation is performed with a purely rectangular pulse without hold level.

4.3 Matching by connecting SSPF in parallel: Experimental results

As the simulation in ADS predicted, a parallel circuit of two SSPF results in nearly step-free transmission of a rectangular pulse. In this section, we present the associated experimental results.

4.3.1 Comparing different parallel setups

We begin with a description of the setups for testing parallel circuit configurations of our SSPF.

Two asymmetric filters

At first a pair of asymmetric 105 cm-filters (pitch: 0.75 mm) is connected in parallel according to the rules found in Ch. 4.2. Each of them has an impedance level of approximately 100 Ω. In the next step, the same is done with a pair of asymmetric 80 cm-filters (pitch: 1 mm, impedance approximately 80 Ω). A parallel circuit built from those devices is expected to have an impedance of 40 Ω.

There are different possibilities to connect two asymmetric filters. The easiest way is using a T-connector. A more sophisticated technique is connecting the filters to a reactive power divider or a resistive power splitter (Wilkinson power splitter). The latter are passive microwave components and at least the power dividers also function as combiners. For this experiment the unidirectional power splitters were used as combiners as well. All three devices have a matching of 50 Ω at each port, but the reactive power divider (Miteq PD2-2000/8000 30S) is specified only in a frequency range of 2 GHz to 8 GHz. The simple T-connector has a limited frequency range and the resistive power splitter (MiniCircuit ZFRSC 42+) is specified from DC to 4.2 GHz.

Two symmetric filters

For connecting two symmetric filters in parallel, which do not have SMA connectors, a PCB with a microstrip T-junction is required. Since the simulations in Sec. 4.2 showed that the details of the board design are unimportant, we decide to use a rectangular design, sometimes with mitered bends. This setup is shown in Fig. 4.5.

Figure 4.5: Sample holder with two symmetric filters in parallel: Two microstrip PCBs with a rectangular mitered T-junction are used to connect the filters in parallel.

Symmetric filters with Kapton closing are the first choice for putting them into a parallel circuit, because their symmetry is much more distinct (cf. Fig. 3.17) and they are much easier to fabricate than filters with Teflon closing.

Filter with integrated parallel circuit

Since the space in a cryostat for flux qubit measurements is typically limited, we finally examine a compact version of impedance matched SSPF. To this end, two single cores, each consisting of only one Stycast rod with a spirally wound wire are mounted inside one casing. At both ends the two cores are soldered together and onto the pin of a SMA connector (cf. Fig. 4.6). As a result the filter with an integrated parallel circuit has the same size as a single conventional asymmetric SSPF.

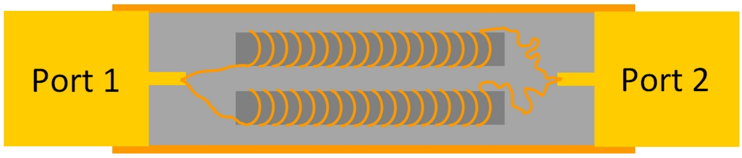

Figure 4.6: Schematic drawing of SSPF with two single cores in parallel: For reasons of fabrication the routing of the wire at port 2 is not well defined, similar to the case of single asymmetric SSPF. Hence asymmetry effects are measurable.

4.3.2 Attenuation characteristic

As a first check, we verify that the attenuation does not degrade when connecting two filters in parallel. In Fig. 4.7 the transmission characteristics of the standard SSPF are compared to the parallel circuits. The overall attenuation behavior is very similar, although the parallel circuits show some additional small structures. The filter with an integrated parallel circuit has two cores with only about 50 cm wire each and, hence, the fall-off reaches the noise floor at 4 GHz. As expected, this is similar to the ∞-wound SSPF 57.3 cm.

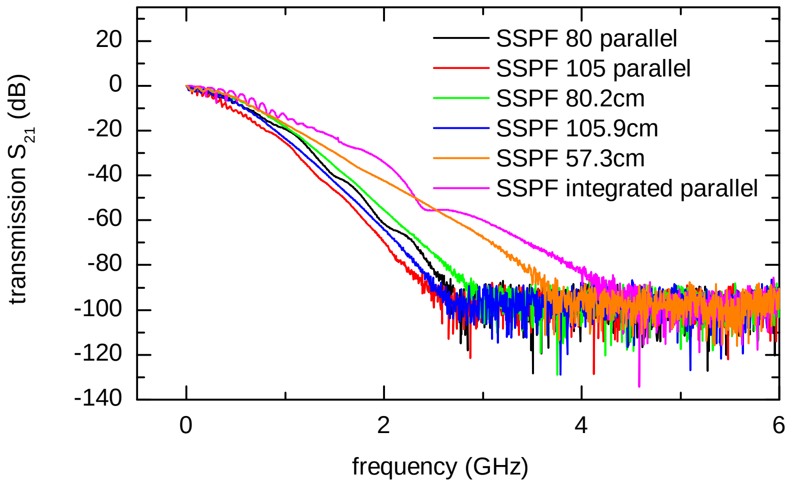

Figure 4.7: Attenuation of parallel filters compared to single filters: SSPF 80 parallel (consisting of SSPF 79.5 cm and SSPF 80.2 cm in parallel, each 80 Ω impedance) and SSPF 105 parallel (SSPF 105.9 cm and SSPF 106.6 cm in parallel, each 100 Ω impedance).

In Fig. 4.8 we can see that the parallel circuit has a lower reflection factor at low frequencies in the passband of the filter. Consequently, the quality of the transmitted pulses is superior to the single SSPF.

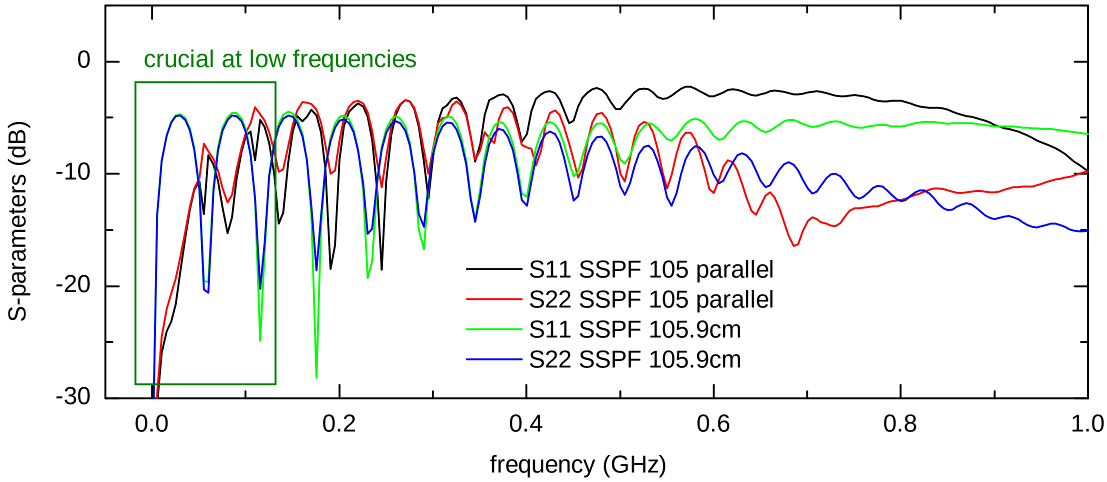

Figure 4.8: S_{11} and S_{22} parameters of SSPF 105.9 cm and a parallel circuit with two 105 cm filters. At low frequencies the parallel circuit has less reflection.

4.3.3 Pulse transmittance

In this section, we analyze in detail the pulse transmission properties of parallel SSPF assemblies. Naively, we expect that a pair of 105 cm filters with a combined impedance of 50 Ω should distort a transmitted pulse less than a pair of 80 cm filters with a combined impedance of 40 Ω. In the experimental traces shown in Fig. 4.9, however, that there is almost no difference visible except the bumpy part on top of the pulse with a characteristic pattern for each pair of filters. In particular, the step is barely visible and superposed by Gibbs ringing.

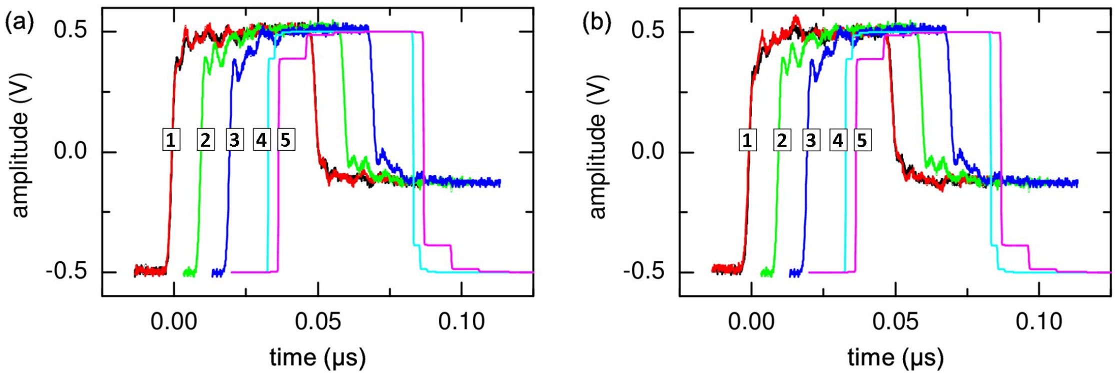

Figure 4.9: Pulse transmission experiment for (a) two asymmetric 80 cm (80 Ω overall impedance) and (b) two asymmetric 105 cm (100 Ω overall impedance) filters in parallel: The curves are for [1] two SSPF, [2] two 26 cm cables [3] two 100 cm cables between two T-connectors. [3] and [4] are the ADS simulations corresponding to [2] and [3], respectively. The graphs are shifted along the time axis by arbitrary offsets for better identification.

Nevertheless, we can show that the mechanism for the impedance matching is the strong reduction of the impedance mismatch in the parallel circuit assemblies. To this end, we compare the parallel assemblies of two SSPF to parallel assemblies of two 50 Ω matched coaxial cables. The latter have an effective impedance of 25 Ω, and two well defined reflection points at either end. As shown in Fig. 4.9, when changing from two parallel SSPF to two parallel 26 cm cables to two parallel 100 cm cables, we can observe the formation of an observable step again. Except for some ringing artifacts, this is also confirmed by ADS simulations. The step height is approximately 11% of the intial total pulse height, as expected for a 50-to-25 Ω impedance mismatch.

Parallel symmetric filters and fabrication pitfalls

As shown in Fig. 4.10(a), a parallel circuit of two symmetric SSPF with Kapton closing causes even less pulse distortion than a parallel circuit of two asymmetric SSPF. After recording this graph, the thin wire stub of one of the Kapton filters in the assembly broke during soldering (the second filter remaining intact). The filter was fixed by cutting it open, pulling a small part of the wire off the core, refilling the spilled powder and closing the filter again. In addition, a third Kapton filter is fabricated, but this time the core length is slightly different from the length of the copper casing causing the core not to abut on the Kapton foil. As shown in Fig. 4.10(b), the transmitted pulse is distorted in a clearly different way for all three Kapton filters. We conclude that the filter performance is very sensitive to details of the fabrication process. In particular, the geometry of the windings on two filters has to be as similar as possible in order to produce an equal behavior with respect to pulse transmission. Furthermore, it is necessary that the core abuts on the Kapton foil, because wire lying undefined in the powder influences the filter characteristic in an uncontrolled way. We note that for a good performance of a parallel circuit of two SSPF, the properties of both filters should ideally be identical.

Power splitters and power dividers

In order to explain the pulse transmission quality of a parallel circuit other couplers than the simple T-connector were used for measurements. Uncontrolled influence on the SSPF is avoided by looking at parallel circuits of 50 Ωmatched cables of different length. In Fig. 4.11 one can see that if the two couplers are directly connected, the step disappears and only the ringing remains (perfect match). As soon as two TRL cables with an impedance of 50 Ω are connected between the ports a mismatch is generated and a step appears. As in Fig. 4.9 longer cables produce a wider step. For a resistive power splitter the amplitude is lower because of the characteristic attenuation of the device. Altogether, we do not observe an improvement by using power splitters or dividers instead of simple T-connectors. The measurements are dominated by the Gibbs ringing pattern, characteristic for square pulses (cf. Sec. 2.2). The ringing is not so clearly visible when looking at the resistive power dividers, because it is attenuated in this case. We conclude

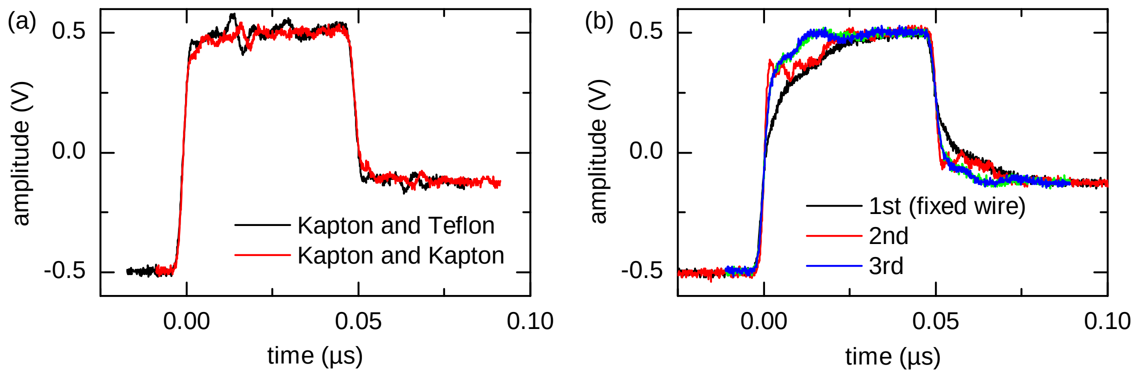

Figure 4.10: (a) Pulse transmission of a combination of two filters with Kapton closing compared to a combination of one filter with Kapton and one with Teflon closing. (b) Pulse transmission of single symmetric SSPF filters with Kapton closing: 1st filter with a repaired wire, 2nd filter normal and 3rd filter. The latter is measured in both directions (blue and green).

that in most cases, the T-connectors are the most convenient method for connecting two filters in parallel.

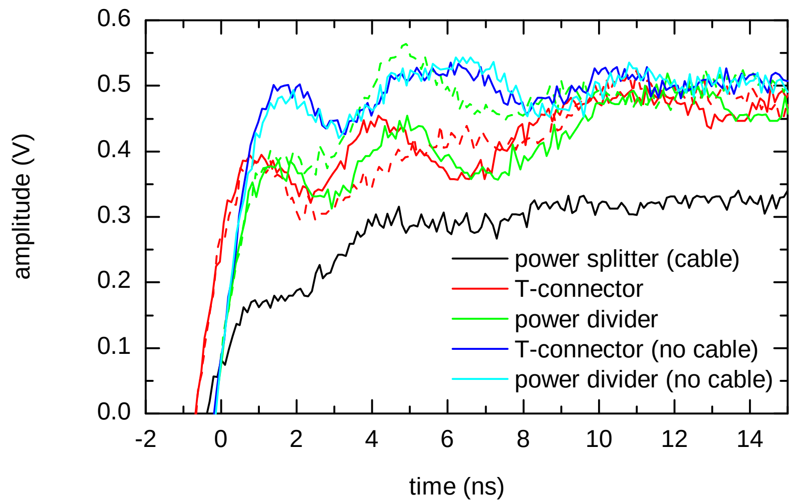

Figure 4.11: Comparison of different couplers introduced in Sec. 4.3.1: Dashed graphs represent shorter cables (26 cm), whereas the green and red solid graphs are with 100 cm cables.

Filter with integrated parallel circuit

In this design, no external couplers are necessary since the wire ends of the two cores are soldered directly to the connectors. As shown in Fig. 4.12, one single core alone has a characteristic step, because its impedance is not matched and therefore causes reflections. The square pulse through a filter with two single cores in parallel, however, cannot be distinguished from a thru device anymore. This means, the filter is perfectly matched and only the Gibbs ringing distorts the signal. Furthermore it seems, that the filter is nearly symmetric, because measurements at both ports show almost the same result. We conclude that the most compact filter clearly shows the best pulse transmission properties.

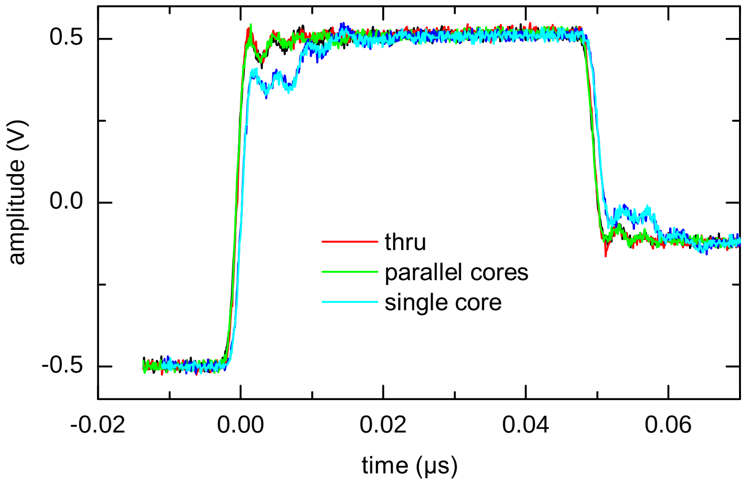

Figure 4.12: Pulse transmission of a filter with two single cores connected in parallel compared to a single core and a thru. After recording this graph, one of the two symmetric SSPF broke, hindering further high-quality results with this configuration.

4.3.4 TDR impedance measurements

We finally confirm the results from Sec. 4.3.3 by means of spatially resolved TDR impedance measurements. We first investigate parallel circuits of asymmetric SSPF. Figure 4.13 shows the TDR response of a filter pair coupled with either a power splitter, a power divider or a T-connector. All three devices show in principle the same response (the shift of the resistive power splitter curve is an artifact due to the power absorbed by the resistive splitter). This confirms our previous result that the performance of the parallel circuit SSPF is independent on the choice of coupling device. Furthermore, one can see that the T-connector is the shortest device, followed by the splitter and then the divider. We note that the narrow dip down to $25\,\Omega$ does not seem to have a large influence on the transmitted pulse.

Symmetric filters

The TDR response of parallel circuits from symmetric filters is not shown here because after recording the high-quality pulse transmission graph from Fig. 4.10(a) one of the filters broke and no equivalent second filter was fabricated.

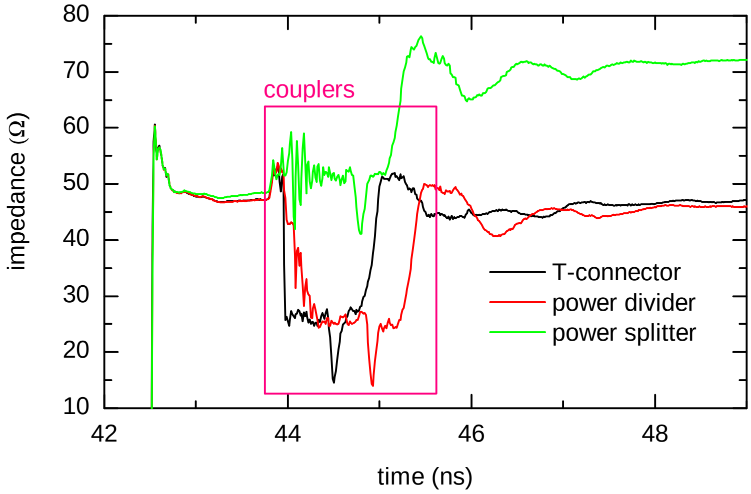

Figure 4.13: TDR response of a parallel circuit of asymmetric filters (SSPF 80.2 cm and SSPF 106.6 cm) with different couplers: On the left of the red box is the TDR step with the initial 50 Ωmatched cable, on the right is the filter.

Filter with integrated parallel circuit

Since the filter with an integrated parallel circuit show excellent transmission properties for square pulses, we can improve our understanding by means of a detailed TDR analysis. First we investigate a single core, which is only one Stycast rod with a spirally wound wire. It is placed in a copper casing, filled with powder and enclosed with a SMA connector on each side. In Fig. 4.14 we see the asymmetry of this filter type caused by the SMA connectors and the fabrication process. The small wiggles indicate that the core is not wound perfectly regular. The most important thing, however, is the impedance level of about 100 Ω, due to the core pitch of 0.75 mm. Connecting two single cores of this kind in parallel is expected to decrease the impedance to 50 Ω in total.

Indeed, when looking at Fig. 4.15, we find that the impedance of the integrated parallel filter is half the impedance of the single core filter. As expected from the fabrication procedure, the TDR response is that of an asymmetric filter due to the longer wire at port 2. A Kapton closing (not realized in the scope of this work) would make the filter symmetric.

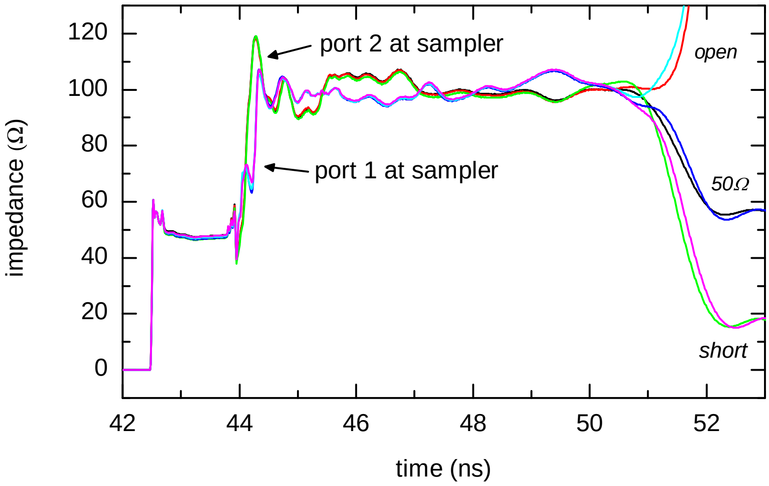

Figure 4.14: TDR data of an asymmetric single core SSPF

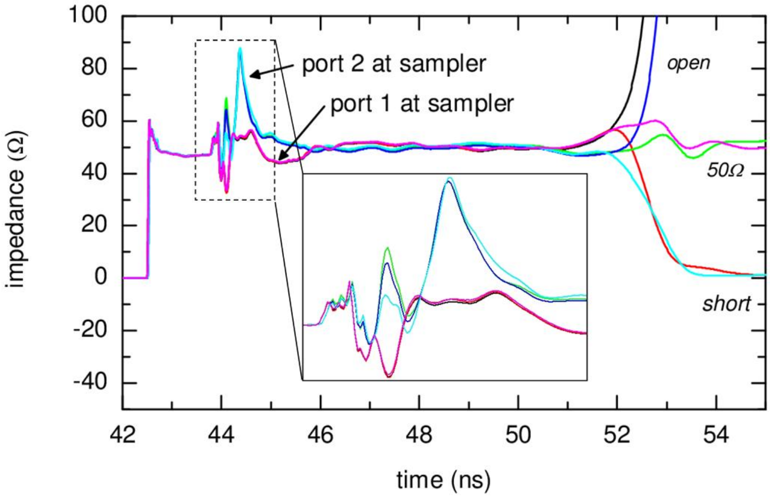

Figure 4.15: TDR data of two single cores in parallel integrated in one casing: The overall impedance is $50\,\Omega$, resulting from two single cores with $100\,\Omega$ connected in parallel. Still there are asymmetry effects, because SMA connectors were used.

Chapter 5

Conclusion and Outlook

In this work, we investigate and improve lowpass SSPF required for the suppression of destructive high-frequency noise in experiments towards solid state quantum simulation and information processing using superconducting flux quantum circuits. The filters are made from an eight-shaped or spirally would copper wire in stainless steel powder. They allow for the passage of current or voltage pulses with 1 GHz bandwidth while, at the same time, attenuating higher frequencies up to tens of gigahertz by more than 80 dB. However, the inner impedance of 80-100 Ω of the SSPF is not matched to the 50 Ω standard for microwave components. The resulting reflections severely distort signals, preventing a controlled pulse design.

Investigating various geometries for the connector-wire transition, we find that the impedance mismatch is not located there but deeper inside the filter. For this reason, we cannot simply apply a matching circuit. Instead, we find that a parallel circuit of two nearly identical SSPF gives almost ideal 50 Ω matching without degrading the filter performance. The improvement in impedance matching is so strong that its effect on a transmitted pulse can be observed directly on an oscilloscope. Finally, we show the first steps towards a more compact design by integrating the parallel circuit inside a single casing.

We emphasize that our impedance matched SSPF preserve the pulse well enough to implement pulse shaping on a one-nanosecond timescale despite the presence of the filter. This paves the way for applying advanced optimum control techniques to improve the fidelity of quantum gates based on superconducting flux quantum circuits. Nevertheless, further improvement of the SSPF is desirable. In addition to systematic studies on fabrication parameters such as the core pitch or the wire properties, one specific improvement could be to combine the integration of the parallel circuit into a single casing with the controlled connector-wire transition (cf. Fig. 5.1). Finally, another interesting approach would be to decrease the pitch and use more than two or single cores in parallel, resulting in a possibly even more compact design.

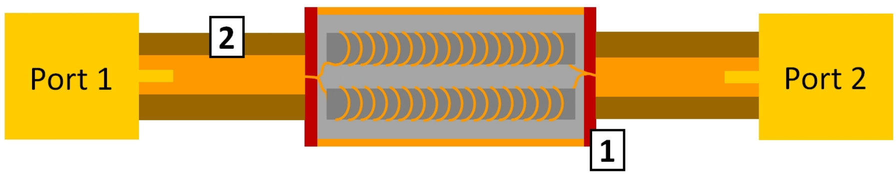

Figure 5.1: Schematic drawing of symmetric SSPF with two single cores in parallel: [1] Kapton foil and [2] microstrip PCB with $50\,\Omega$ impedance strip. A generalization to more than two single cores is straightforward.

Appendix A

Instructions for fabricating SSPF

In this section, we present a short recipe-like manual with helpful hints in the construction process of a SSPF.

A.1 Building a SSPF with Kapton foil on both ends

Manufacturing the Stycast-powder rods:

- Mix Stycast 1266 (A:B = 100:28) in a small plastic jar.
- Add stainless steel powder (Stycast:stainless steel powder = 1:4.016) and stir well with a toothpick.
- Place the plastic jar in a desiccator and evacuate it. Be careful not to let the mixture spill out of the jar. As soon as the mixture stops bubbling, vent the desiccator. Repeat this procedure at least two times. Do not leave the mixture inside the desiccator too long, because it turns too viscous after an hour.
- Use a toothpick to fill the mixture into a plastic syringe. Avoid air to settle in the mixture.
- Press the mixture into a Q-tip tube and let it harden. Do not use a needle.
- Use a scalpel to cut open the Q-tip tube. Be careful not to break the Stycast rod.
- Carve a thread with a pitch of 0.75 cm onto the Stycast rod. A pair of rods should have one right-handed and one left-handed thread. This is conveniently done on a lathe in the workshop.

Manufacturing cores for the filters:

- Put a carved pair of rods into the plastic holder and wind a 200 μm copper wire in ∞-form onto a pair of rods. Leave at least 3 cm of wire at both ends.
- Make sure that the rods are exactly as long as the copper casing and are plane at their ends.

- Use a thin needle to pierce two pieces of Kapton foil 125 μm, which are large enough to close the casing.

- Thread one piece of Kapton foil onto one side of the wire and place the wound pair of rods into a copper casing.

- Mix Stycast 1266 and use it to glue the Kapton foil with the pair of rods onto the copper casing. Let the Stycast harden.

Filling the filters with powder:

- Mark port 1 and port 2 of the filter. This is useful for the measurements afterwards.

- Place the copper casing with the open end on top into a holder and affix a ring of sticky tape at the open end.

- Use a small funnel to fill in the stainless steel powder.

- Place the holder onto a vibrating apparatus in order to densify the powder.

- Thread the second piece of pierced Kapton foil onto the copper wire on the open side and glue it onto the copper casing. Let the Stycast harden.

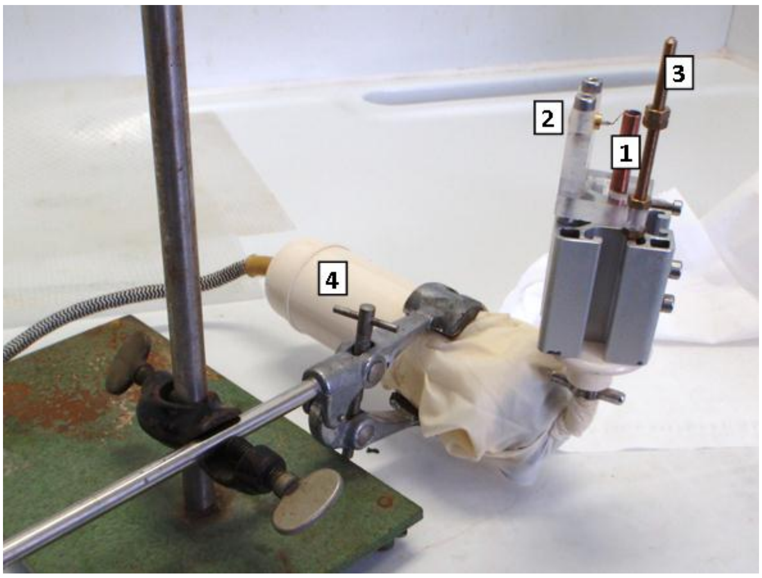

Figure A.1: Filling process with vibrating apparatus to densify the powder: [1] copper casing with core inside and first SMA connector at the bottom and [2] second SMA connector soldered onto the core wire. [3] holder for a funnel and [4] vibrating apparatus. The filling process is analogous for symmetric filters with Kapton closing, except for the absence of the SMA connectors.

Placing the filter into the sample holder:

- Cut the copper wire on both ends and leave about 2mm for soldering.
- Cut the overlaying Kapton foil with a small pair of scissors and grind off the rest carefully with a low speed grinding machine.
- Use two appropriate printed circuit boards and two flange mount SMA connectors (Rosenberger 32K724-600S5 Panel Jack Stripline) and solder everything together in the sample holder. Be careful never to break the wire when soldering.

A.2 Building an asymmetric SSPF with SMA connectors on both ends

- For an asymmetric SSPF you can use the procedure for the symmetric filters described in App. A.1. However, instead of using thin Kapton discs, solder a SMA connector (Huber+Suhner 22_SMA-50-0-15/111_N Coaxial Panel Connector) on the core wire and glue it into the copper casing.
- Fill the filter as described in App. A.1.
- Close the filter by soldering the second SMA connector onto the free end of the core wire. Use a bit of Stycast to seal the filter. Make sure that the copper casing has a conducting connection to the connector casing.

Appendix B

Devices for controlling the connector-wire transition

In this section, we characterize various PCB for a controlled connector-wire transition. We are aware that most of these PCB do not actually act as matching circuits. Their purpose is to find out whether it is possible to "pull" the mismatch out of the filter for later treating it with an appropriate matching circuit.

Despite the fact that the successful impedance matching strategy has turned out to be a different approach (cf. Ch. 4), we keep this data as an appendix because it gives valuable insight into practical high frequency design.

B.1 Microstrip PCB

A microstrip waveguide or, short, microstrip is a conductive strip etched on a substrate (cf. Fig. B.1) with a conductive ground plane on the back side [9]. The impedance of the microstrip can be changed by altering its width.

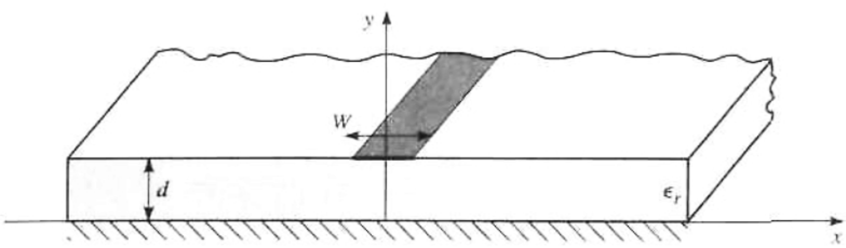

Figure B.1: Microstrip transmission line geometry [9]

Design

Using the software txline2003 from AWR [13] one can easily calculate the widths corresponding to $50\,\Omega$ and $80\,\Omega$ from the specifications of the substrate (thickness of the metallic layer, the dielectric constant ϵ_r, height). Our substrate is RT5870 (ROGERS Corporation) with ϵ_r=2.33, an height of 0.508 mm and a copper thickness of 18 µm. Boundary effects are not considered in the calculation in txline2003, as a result the formula can be given as in [9].

$$\frac{W}{d} = \begin{cases} \frac{8e^A}{e^{2A}-2} & \text{for } W/d < 2 \\ \frac{2}{\pi}\left[B - 1 - ln(2B-1) + \frac{\epsilon_r - 1}{2\epsilon_r}\left\{\ln(B-1) + 0.39 - \frac{0.61}{\epsilon_r}\right\}\right] & \text{for } W/d > 2 \end{cases} \tag{B.1}$$

$$\begin{aligned} A &= \frac{Z_0}{60}\sqrt{\frac{\epsilon_r + 1}{2} + \frac{\epsilon_r - 1}{\epsilon_r + 1}\left(0.23 + \frac{0.11}{\epsilon_r}\right)} \\ B &= \frac{377\pi}{2Z_0\sqrt{\epsilon_r}} \end{aligned}$$

Impedance	calculated width of strip
50 Ω	1.488893 mm
80 Ω	0.661685 mm

In order to fit into a sample holder the microstrip board is 4 mm wide and 6 mm long. A linear design is chosen and a mask for etching is modeled with Corel Draw.

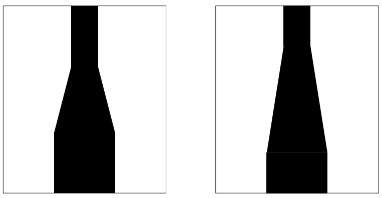

Figure B.2: Layouts of two microstrip PCB (4 mm x 6 mm) with different slopes: Left M (medium), right L (long). Black parts are conductive.

B.2 T-attenuator

A T-attenuator (TA) consists of three resistors and transforms the impedance from Z_{in} to Z_{out} depending on the values of the resistors.

A characteristic quantity of a TA is the attenuation N.

$$N = \sqrt{\frac{P_{in}}{P_{out}}} = \sqrt{\frac{I_S^2 R_1}{I_R^2 R_2}} = \frac{I_S}{I_R}\sqrt{\frac{R_1}{R_2}} \tag{B.2}$$

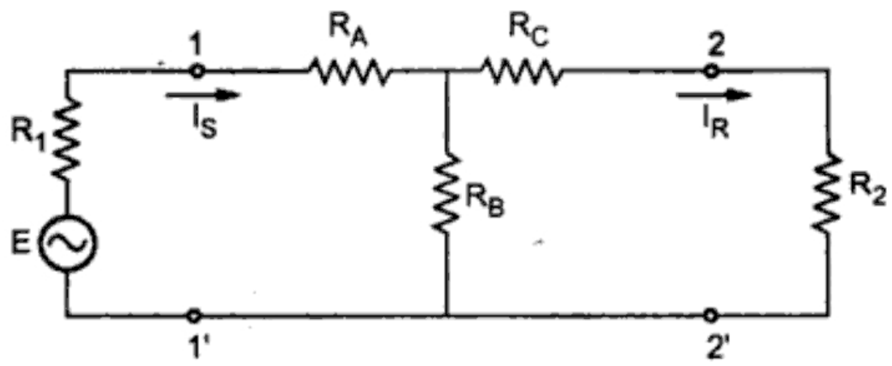

Figure B.3: T-attenuator circuit diagram [14]

The values of interest are R_A, R_B and R_C, whereas R_1 is $50\,\Omega$ and R_2 is the desired impedance. From [14] we get the following formulas.

$$R_A = R_1 \left[\frac{N^2+1}{N^2-1}\right] - 2\sqrt{R_1 R_1}\left[\frac{N}{N^2-1}\right] \quad \text{(B.3)}$$

$$R_B = 2\sqrt{R_1 R_1}\left[\frac{N}{N^2-1}\right] \quad \text{(B.4)}$$

$$R_C = R_2 \left[\frac{N^2+1}{N^2-1}\right] - 2\sqrt{R_1 R_1}\left[\frac{N}{N^2-1}\right] \quad \text{(B.5)}$$

We choose the desired impedance R_2 to be $80\,\Omega$, in order to match filters with an impedance of $80\,\Omega$. Moreover a symmetric TA is fabricated for further studies.

TA		R_A/Ω	R_B/Ω	R_C/Ω	fwd attenuation/dB	rev attenuation/dB
symm.	$50\,\Omega \to 50\,\Omega$	22	47	22	8.1	8.1
asymm.	$50\,\Omega \to 80\,\Omega$	56	56	10	8.6	8.9

In order to connect the asymmetric TA device to the filter and the SMA connector with the right impedance, a board with $50\,\Omega$ impedance on one side and $80\,\Omega$ on the other is needed. It is the easiest to realize this with microstrip (for widths see Sec. B.1).

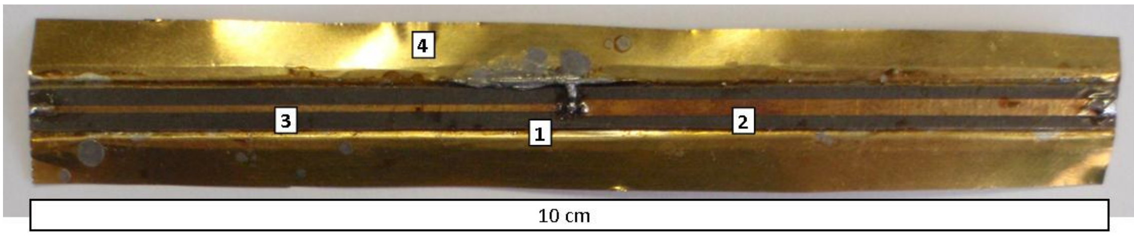

Figure B.4: TA device soldered on a long microstrip: [1] resistors in T formation, [2] microstrip with 50 Ω impedance [3] microstrip with 80 Ω impedance and [4] brass sheet for grounding.

B.3 Coplanar waveguide

A coplanar waveguide (CPW) consists of a narrow center strip separated from two (theoretically infinitely large) ground planes by a gap on each side. Ideally, the opposite side of the substrate is not conductive (cf. Fig. B.5). The dimensions for characteristic impedances of 50 Ω and 80 Ω are determined using the software txline2003 [13]. Analytical formulas can be found in standard literature on transmission lines, e.g. [15]. The structures are fabricated on a ROGERS RO 3010 substrate (ϵ_r=10.2, 0.635 mm height, 18 µm copper).

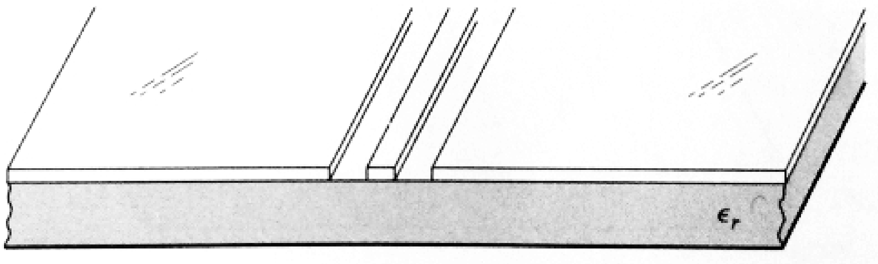

Figure B.5: Coplanar waveguide transmission line geometry [9]

Impedance	calculated width of strip	calculated width of gap
50 Ω	0.964425 mm	0.35 mm
80 Ω	0.507694 mm	0.87 mm

Figure B.6: Layout of CPW boards (4 mm x 6 mm) with a 50 Ω to 80 Ω impedance transition. Left M (medium), right L (long). Black parts are conductive.

B.4 Analysis of PCB structures

The same three measuring methods for the SSPF, TDR spectroscopy, S-parameter and pulse transmission analysis, are applied to the microstrip PCB, the CPW PCB and the TA.

B.4.1 Attenuation

As expected for a transmission line made of a good conductor, the transmission characteristics of the microstrip and CPW boards are qualitatively similar to those of a coaxial cable (cf. Fig. B.7). The broad resonances at high frequency in the CPW boards are most likely caused by the PCB geometry. In the passband of the SSPF, all boards can be considered as thru devices.

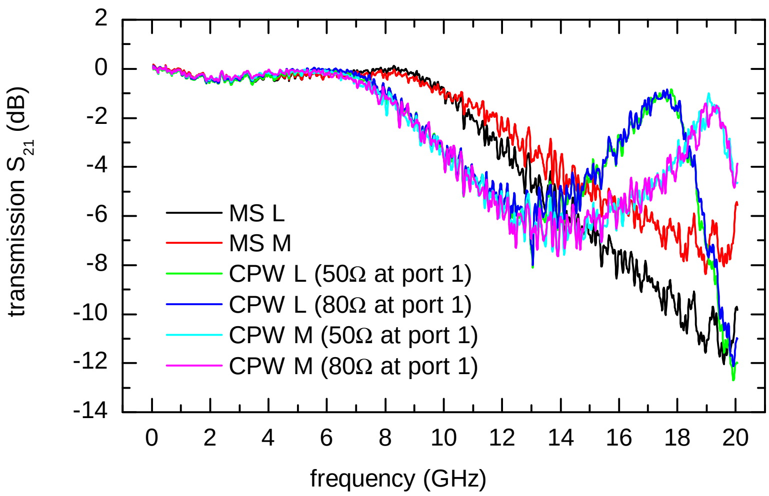

Figure B.7: Attenuation of microstrip and CPW PCB from 0 to 20 GHz.

The TA exhibits an attenuation by design (data not shown). If R_1 and R_2 are the same, the forward and reverse attenuation is the same, otherwise we have to distinguish a forward and reverse attenuation.

B.4.2 Pulse transmittance

The same measurement of a transmitted pulse done with the filters (cf. Sec. 2.2) can be performed with the transmission lines alone.

As shown in Fig. B.8, the transmitted pulse shows no distortion. One reason for this is the short length of the PCB, resulting in a time delay of only 0.11 ns between the pulse and a possible ghost pulse. The asymmetric TA attenuates the pulse as expected.

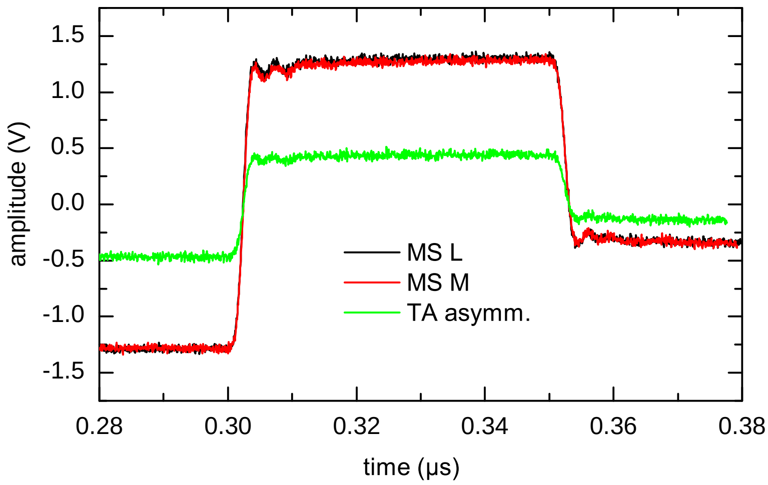

Figure B.8: Transmitted pulse through microstrip PCB and TA.

B.4.3 Impedance

TDR spectroscopy is the most interesting measurement for these devices, because it shows the spatial dependence of the impedance. An ideal graph would have a smooth change from 50 Ω to 80 Ω.

Short boards

At first short boards with a length of 6 mm are taken for measurement. In Fig. B.9 the impedance of a microstrip and a CPW PCB is shown. Different from the naive expectation, the TDR response is dominated by two peaks due to the connector-PCB connection.

In other words, all those boards are too short to resolve the impedance characteristic of the transmission lines. Moreover soldering a 50 Ω matched connector onto the 80 Ω strip causes further problems.

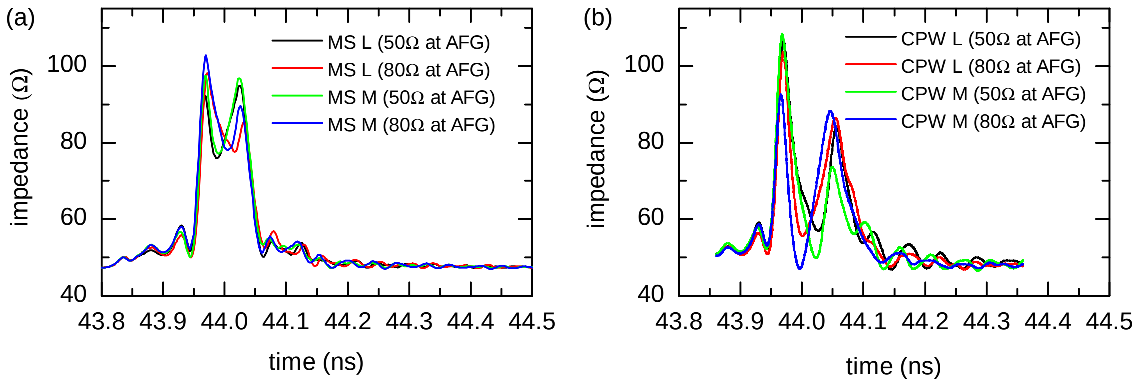

Figure B.9: TDR response of short microstrip (MS) and CPW PCB with a 50 Ω-to-80 Ω transition.

Long boards

As a result to the problems occurring with short boards, a longer microstrip PCB is designed (cf. Fig. B.10). It has 50 Ω impedance at both ends in order to match the SMA connectors and has a longer 80 Ω matched section in the middle. The attenuation and pulse transmission characteristics are comparable to the short boards. As shown in Fig. B.10, we fabricate boards with two different transition lengths (”slopes”) between the 50 Ω and the 80 Ω matched sections.

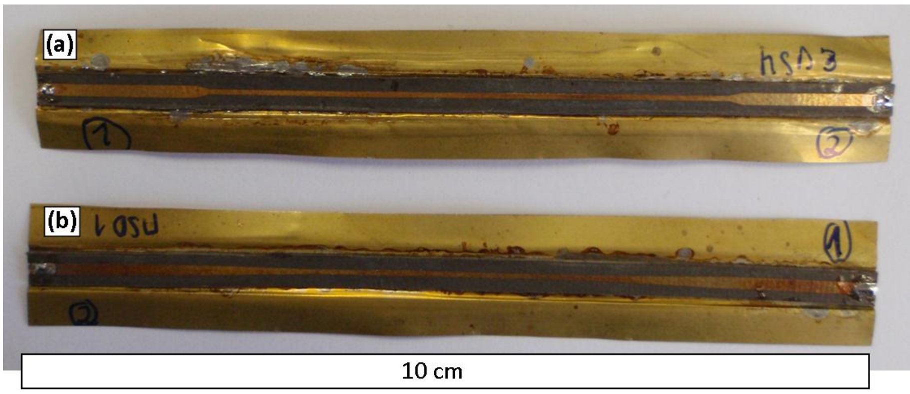

Figure B.10: Microstrip on long board: (a) with short slope and (b) with long slope. The brass sheet, onto which the boards are soldered, is for grounding.

Board type	slope
Microstrip-LS (long slope)	15 mm
Microstrip-SL (short slope)	1.6 mm

In the TDR response shown in Fig. B.11, the peaks due to the two SMA connectors on the left and the right with their soldering joints are again clearly visible. The transition between the 50 Ω and the 80 Ω regions are much steeper for the ”short slope” board than for the ”long slope” board and correlate with the slope length. We can conclude that the change in impedance is indeed smooth as expected.

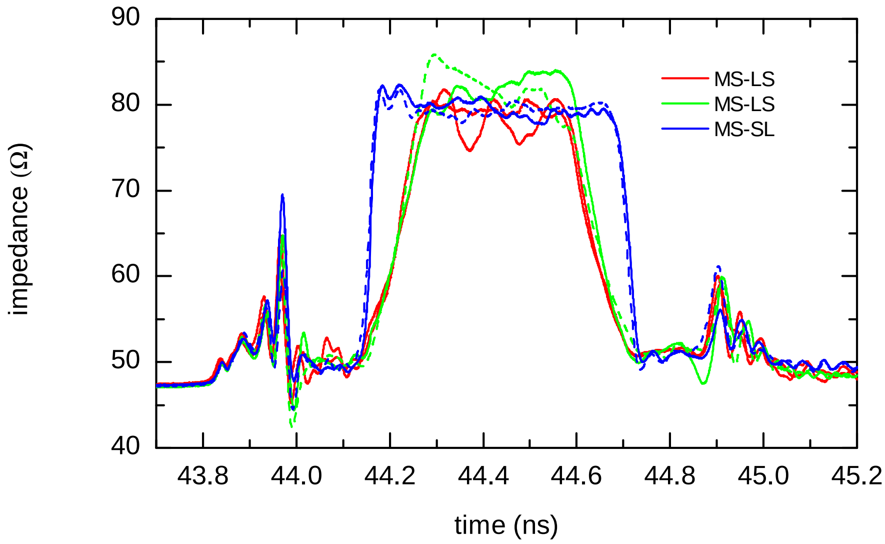

Figure B.11: TDR data of long microstrip boards with different slopes. The dashed graphs show the boards reversely connected to the TDR sampler and the asymmetry comes from inaccurate etching.

Connector-board transition

Taking a closer look at the connector-board transition, another type of connector is tried (Rosenberger 32K724-600S5 Panel Jack Stripline). It is flange-mounted and has a short stripline instead of a soldering pin and hence a smaller soldering joint is possible. In Fig. B.12 the TDR response of the relevant region is shown. A smaller soldering joint results in a slightly lower impedance, because the effective thickness of conductive material is decreased. Furthermore the flange-mounted connector has its own distinct impedance pattern. Again it is possible to determine the lengths of the measured structures. Using Eq. (2.12) and the TDR data, we obtain 2.1 cm for the board length in good agreement with its real length of 1.8 cm.

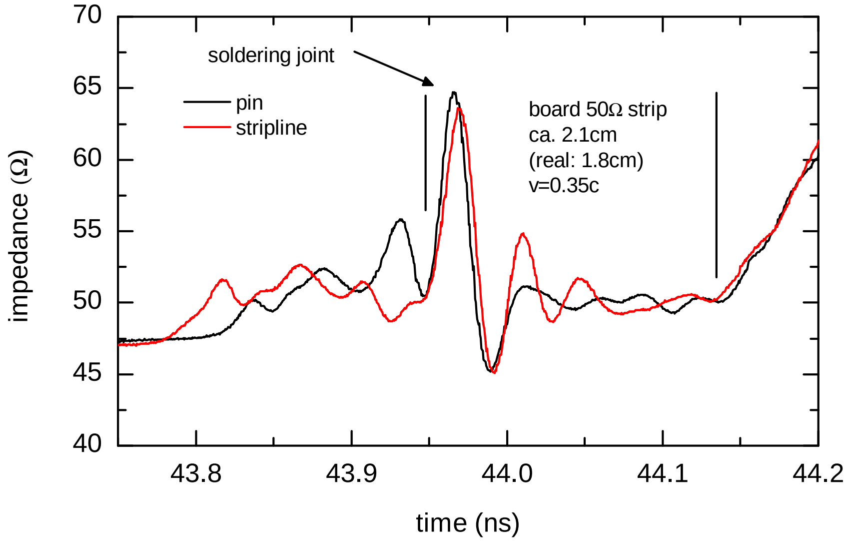

Figure B.12: TDR data of the connector-board transition for two different SMA connectors.

Appendix C

TDR data examples

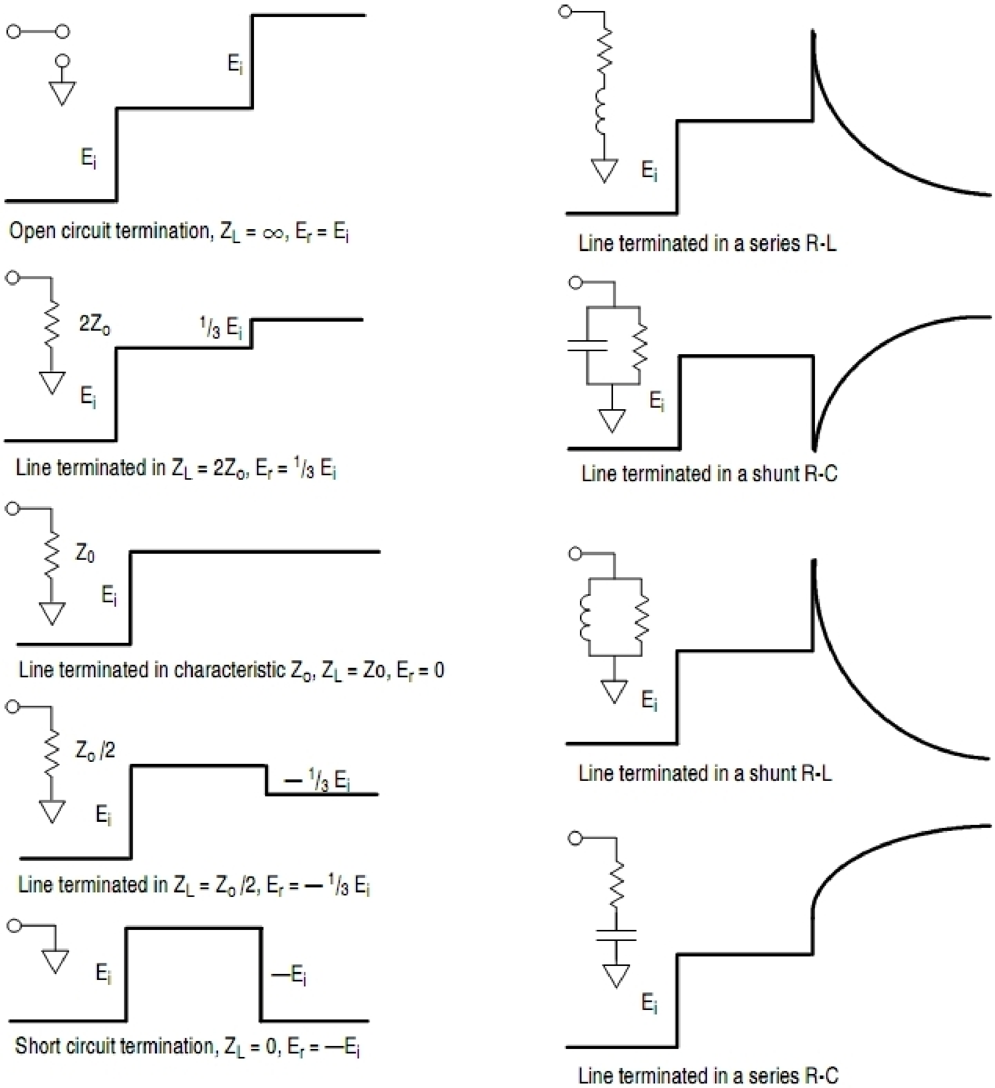

Figure C.1: Examples for TDR data: These nine examples show different loads and their influence on the reflected voltage. The graphs are superpositions of the incident signal E_i and the reflected signal E_r. [16]

Bibliography

[1] Fukushima, A. et al.: *Attenuation of microwave filters for single-electron tunneling experiments.* 46(2):289–293, 1997.

[2] Lukashenko, A et al.: *Improved powder filters for qubit measurements.* Review of Scientific Instruments, 79(1):014701, 2008.

[3] Forn-Diaz, P. et al.: *Josephson squelch filter for quantum nanocircuits.* Applied Physics Letters, 95(4):042505, 2009.

[4] Spietz, L. et al.: *A Twisted Pair Cryogenic Filter*, 2008.

[5] Santavicca, D. F. et al.: *Impedance-matched low-pass stripline filters.* Measur.Sci.Tech., 19, 2008. To appear in Measurement Science and Technology.

[6] Deppe, F. et al.: *Phase coherent dynamics of a superconducting flux qubit with capacitive bias readout.* Phys. Rev. B, 76(21):214503, Dec 2007.

[7] Phillips, C.L. et al.: *Signals, systems, and transforms.* Prentice Hall, 2008.

[8] Fisher, R. et al.: *Optimal control of circuit quantum electrodynamics in one and two dimensions.* Phys. Rev. B, 81(8):085328, Feb 2010.

[9] Pozar, D. M.: *Microwave Engineering.* John Wiley & Sons, Inc., 2nd Edition , 1998.

[10] Agilent: *Advanced Design System (ADS) 2009.*

[11] Deppe, F.: *Superconducting flux quantum circuits: characterization, quantum coherence, and controlled symmetry breaking.* , TU München, 2009.

[12] Hartung, J.: *Statistik.* Oldenbourg Wissenschaftsverlag, 2005.

[13] AWR: *TX-Line Transmission Line Calculator.*

[14] Bakshi, A.V. et al.: *Networks and Lines.* Technical Publications, 2008.

[15] Simons, R.: *Conventional Coplanar Waveguide. Coplanar Waveguide Circuits, Components, and Systems*, 11–86. IEEE, 2002.

[16] Tektronix, Inc., 14200 SW Karl Braun Drive P.O. Box 500 Beaverton, OR 97077 USA: *User Manual 80E07, 80E08, 80E09, and 80E10 Electrical Sampling Remote Modules.*

Acknowledgment

In the first place I want to thank my parents, who make it possible for me to study physics. It is their hard work and the grace of God, that I am what I am.

I am indebted to the director of the WMI, *Prof. Dr. R. Gross*, for giving me the opportunity to write my thesis in the qubit group at the WMI.

The most helpful advice was from *Dr. F. Deppe* and *M. Schwarz*, who supervised my experiments and proofread this thesis. Particularly *Dr. F. Deppe* supported me from afar regarding this thesis, while I spent one term abroad.

Special thanks go to *M. Haeberlein* for a tutorial in LabVIEW, to *E. Menzel* for introducing me into the TDR spectroscopy, and to *M. Schwarz* again for the instruction to basic experimental techniques, including the fabrication of filters.

I am grateful to *Dr. C. Morhart* from the faculty of Electrical Engineering at TUM for explaining the simulation tool ADS to me and letting me do the simulations on one of their workstations.

Furthermore I want to mention *R. Müller* from the workshop at the WMI, who helped me in technical questions and manufactured a lot of components for me, and *K. Helm-Knapp*, who instructed me in the etching process and always had time to answer my questions concerning chemistry. Essential parts of the experiments could not have been carried out without the help of the technical staff at the WMI. So I express my gratitude to them.

Last but not least I thank all my friends, physicists and non-physicists, who checked this thesis for linguistic mistakes and supported me in various ways.